Earth-Science Reviews 185 (2018) 938–955

Contents lists available at ScienceDirect

Earth-Science Reviews

journal homepage: www.elsevier.com/locate/earscirev

Three-dimensional evolution of the Yangtze River mouth, China during the Holocene: impacts of sea level, climate and human activity

Zhanghua Wang[a,b,*], Yoshiki Saito[c,d], Qing Zhan[e], Xiaomei Nian[a], Dadong Pan[a], Long Wang[a], Ting Chen[a], Jianlei Xie[e], Xiao Li[e], Xuezhong Jiang[a]

[a] State Key Laboratory of Estuarine and Coastal Research, ECNU, Shanghai 200062, China
[b] Institute of Urban Development, East China Normal University, Shanghai 200062, China
[c] Estuary Research Center, Shimane University, 1060, Nishikawatsu-cho, Matsue 690-8504, Japan
[d] Geological Survey of Japan, AIST, Central 7, Higashi 1-1-1, Tsukuba 305-8567, Japan
[e] Shanghai Geological Survey, Shanghai 200072, China

ARTICLE INFO

Keywords:
Morphodynamic evolution
Coastal erosion
Tidal ridge-and-trough topography
Sediment trapping rate
System regime shift

ABSTRACT

The Yangtze (Changjiang) mega-delta, China, has a high risk of coastal erosion owing to the recent high rate of relative sea-level rise and reduced sediment supply. The study of the Holocene evolution of the delta can provide information about its response to rapid sea-level rise and changes in sediment supply caused by climate or human activity, although this has yet to be fully explored because of the lack of integrated studies using age-constrained sedimentary records. Here we document stratigraphic architecture and morphological changes over the last 11,700 years and estimate the amount of sediment trapped in the delta region on a millennial scale using a dataset of 344 sediment cores, 658 radiocarbon and 28 optically stimulated luminescence (OSL) ages (of which we obtained 64 cores, 345 radiocarbon and 28 OSL ages, and the others we sourced from the literature). Using this dataset we present the temporal and spatial morphodynamic evolution of the entire Yangtze River mouth from its early Holocene transgressive estuary to a mid- to late-Holocene regressive delta, making it possible to produce a quantitative and sequential analysis of sediment deposition. A destructive phase of the river mouth region was identified at 10 to 8 cal. kyr BP, including significant coastal erosion of tidal flats and troughs within the estuary and of tidal ridge-and-trough topography offshore; these resulted from the reshaping of the river mouth morphology caused by rapid sea-level rise at that time. As a result, the rate of sediment trapping at the river mouth declined from an average of 224 Mt yr^{-1} at 11.7–10 cal. kyr BP to 137 Mt yr^{-1} between 10 and 8 cal. kyr BP. Since delta initiation 8000 years ago, a retreat of the subaqueous delta occurred and the sediment trapping rate declined from 151 Mt yr^{-1} at 8–6 cal. kyr BP to 99–113 Mt yr^{-1} between 6 and 2 cal. kyr BP, caused by the reduction in sediment supply linked to summer monsoon weakening ~6000 years ago. In the last 2000 years the sediment trapping rate has increased to 162 Mt yr^{-1} due to intensified human activity. The present-day level of sedimentation in delta (49 Mt yr^{-1} in 2003–2011), after the completion of the Three Gorges Dam, is far lower than the 'natural' range in the Holocene. We thus infer a potential for system regime shift in terms of coastal erosion and a transition to a new equilibrium in delta morphology in the near future.

1. Introduction

The balance between sea-level rise and sediment supply is the major factor controlling the evolution of the sediment deposition system at the interface between rivers and the sea (Stanley and Warne, 1994). Global sea-level rise is predicted to accelerate in the 21st century and could rise 65 ± 12 cm by 2100 compared to a 2005 baseline (Kopp et al., 2016; Nerem et al., 2018). This predicted sea-level rise, together with sediment shortages caused by human activity, is threatening the security of river deltas worldwide in terms of coastal erosion and inundation; this has caused great concern within the the scientific community, leading to major proposals for delta protection (Syvitski et al., 2009; Giosan et al., 2014). For example, the Nile Delta changed from a constructive to a destructive phase over past two centuries due to severe reduction in sediment input and relative sea-level rise (Stanley and Warne, 1998). Land loss induced by sediment starvation also occurs in

* Corresponding author at: State Key Laboratory of Estuarine and Coastal Research, Institute of Urban Development, East China Normal University, Shanghai 200062, China.
E-mail address: zhwang@geo.ecnu.edu.cn (Z. Wang).

https://doi.org/10.1016/j.earscirev.2018.08.012
Received 31 October 2017; Received in revised form 22 August 2018; Accepted 24 August 2018
Available online 01 September 2018

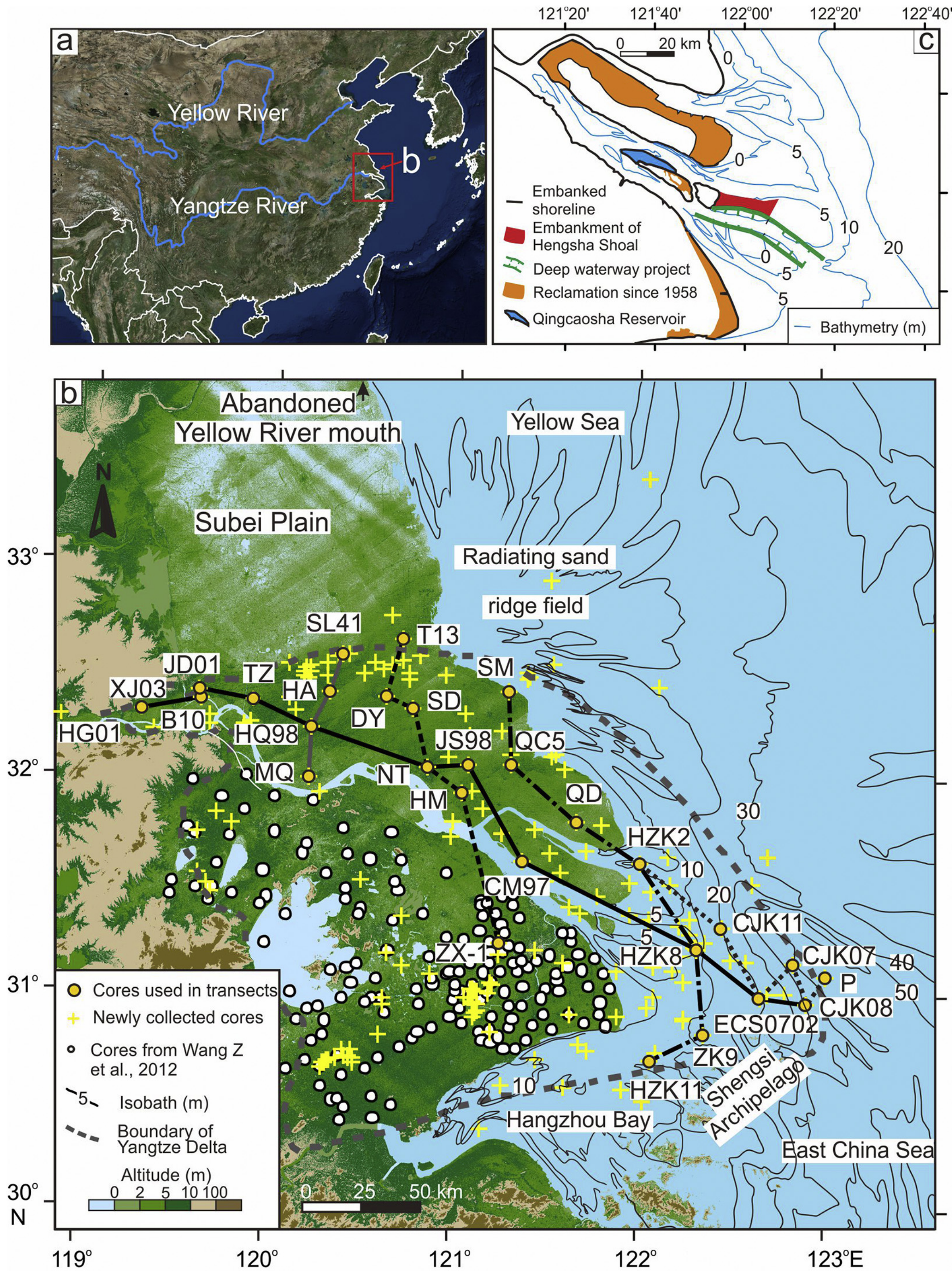

Fig. 1. Location maps. a, Yangtze River catchment. b, the Yangtze Delta showing sediment core sites and the distribution of five stratigraphic cross-sections (heavy black lines) across the Yangtze Delta. The dataset of newly collected sediment cores including those drilled by this study is presented in Table S1. The delta apex was recognized in core HG01 (Song et al., 2013). The base map was generated with the ArcGis 10.1 software (www.esrichina.com.cn) using the topographic dataset provided by the International Scientific & Technical Data Mirror Site, Computer Network Information Center, Chinese Academy of Sciences (http://www.gscloud.cn). c, Major coastal engineering in the present-day Yangtze River mouth includes intertidal reclamation and embankment since 1958; the Qingcaosha Reservoir, which was finished at the end of 2010; and the ongoing embankment of the Hengsha Shoal.

the Mississippi Delta (Coleman et al., 1998) and scientists have called for restoration of the Delta following the lessons learned about the delta plain's deterioration caused by Hurricanes Katrina and Rita (Day Jr et al., 2007). They suggest that the river needs to be reconnected to the delta plain to provide sediment for accretion so that it can keep pace with local sea-level rise. This will also help defend the Delta against storms (Day Jr et al., 2007) which are increasing in both energy and frequency owing to the warming climate and global sea-level rise (Woodruff et al., 2013).

The Yangtze (Changjiang) Delta, China (Fig. 1) is another typically vulnerable delta, given that the megacity of Shanghai, with > 24 million inhabitants, is located there. Erosion in the subaqueous delta has been reported in recent years (; Li et al., 2015), and is thought to be due to a large decline Yang et al., 2011in sediment supply, from ~500 Mt yr^{-1} in the 1950s–1970s to < 150 Mt yr^{-1} after 2003, following construction of > 50,000 reservoirs including the Three Gorges Dam (TGD;

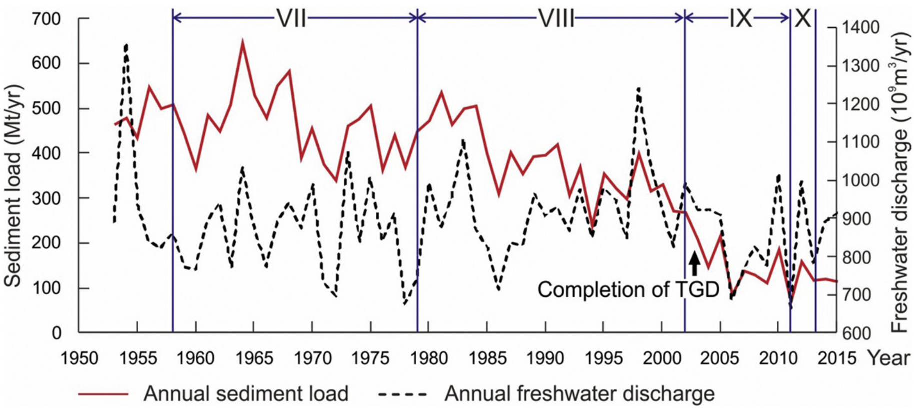

Fig. 2. Annual sediment load and freshwater discharge at Datong Station in the lower Yangtze River between 1953 and 2013. Numbers VII–X represent stages of the sediment budget for recent decades used in Table 2. Note the severe decline in sediment load since completion of the TGD (Data source: Changjiang Water Resources Commission of the Ministry of Water Resources, http://www.cjw.gov.cn/zwzc/bmgb/).

Fig. 2). There is ongoing debate as to how the delta will respond to the recent decline in sediment supply (Dai et al., 2014). Since the extremely high sediment load of the 1950s–1970s is thought to be closely related to significant deforestation during that period (Lu and Higgitt, 1998), it is sometimes assumed that the post-dam reduced sediment load could be similar to the load before those land use changes. Attention has therefore turned to what the ‘natural’ rate of sediment supply would have been during an earlier period when human impacts were weak, such as the early and mid-Holocene.

On the other hand, intensive coastal engineering has greatly changed the morphology and hydrodynamics of the Yangtze River mouth through the reclaimation of the tidal flats, embankment of the mouth shoal and channel deepening (Fig. 1c) (Du et al., 2016). Shoreline “hardening” and associated steepening of the coastal cross-section caused by these engineering projects will amplify tides in a situation of sea-level rise (cf. Holleman and Stacey, 2014; Ensing et al., 2015). It is thus important to examine the Delta's present-day human-impacted status and future trajectory by understanding the long-term morphodynamic evolution of the River mouth, specifically its response to sea-level rise and changes in terrestrial input through the Holocene.

There have been numerous investigations focusing on the Holocene evolution of the Yangtze Delta and its linkage to climate change, sea-level fluctuation, and human activity over the past few decades (cf. Li and Zhang, 1996; Chen et al., 2000; Li et al., 2000; Hori et al., 2001; Wang et al., 2010; Liu et al., 2010; Wang et al., 2011; Zhan et al., 2012; Xu et al., 2013, 2016; Zhang et al., 2017). It has been reported that a tide-dominated estuary was present in the paleo-incised Yangtze valley when sea level rose rapidly during the early Holocene (Li et al., 2000; Hori et al., 2001). Delta sediments began to accumulate when sea-level rise decelerated at ca. 8 cal. kyr BP (Song et al., 2013; Wang et al., 2013). But a recent study argued that a back-stepping delta system developed in the paleo-incised Yangtze valley owing to the huge amount of sediment supplied by the River, which allowed sedimentation in the river mouth to keep pace with or even exceed the rate of relative sea-level rise during the late Pleistocene to early Holocene (Zhang et al., 2017). This argument was primarily based on the lack of an estuarine mouth shoal and a fining-seaward distribution of sediments during the early Holocene (Hori et al., 2001; Zhang et al., 2017). However, early Holocene tidal ridges have been reported in the shelf area near the Yangtze River mouth (Fig. 3; cf. Feng et al., 2017), and there is a strong possibility that a limited number of sediment cores taken in such a large river mouth could miss any early Holocene tidal sand bars in the estuary.

In addition, a number of papers have documented shelf inundation and landward shift of the river mouth for many rivers in the world, including the Yangtze, as a coastal response to rapid sea-level rise during the early to mid-Holocene (Hori et al., 2002a; Tanabe et al., 2006; Hori and Saito, 2007; Tamura et al., 2009; Tjallingii et al., 2010; Zhan et al., 2012; Zong et al., 2012; Song et al., 2013; Tjallingii et al., 2014). A reduction in freshwater discharge and sedimentation at river mouths was also reported as a response to to the weakening of the mid-Holocene Asian Summer Monsoon (ASM) after ~6 cal. kyr BP (Zong et al., 2006; Zhan et al., 2012; Hu et al., 2013; Nageswara Rao et al., 2015). Sedimentary hiatuses have been observed in the post-glacial stratigraphic sequence of the Yangtze coast and many of these are believed to be generated by tidal current and storm wave erosion (Li and Zhang, 1996). We suggest that during periods of rapid sea-level rise or decline in terrestrial input, compensating-adjustment of morphologic and hydrodynamic processes leads to a new equilibrium state between deposition and erosion at the river mouth. Understanding this compensating-adjustment, particulary the erosional processes and their mechanism during the system transition to a new equilibrium, will provide practical insight for coastal management for both the present day and the near future.

In this study, we compiled sediment core data, including lithology, stratigraphy, chronology, and marine microfossils, from previous studies (cf. Li et al., 2000; Hori et al., 2001; Liu et al., 2010; Song et al., 2013; Wang et al., 2010, 2011; 2012; 2013; Xu et al., 2013, 2016; Zhang et al., 2017). Together with our 64 newly obtained sediment cores, 345 radiocarbon and 28 OSL ages (of which 24 OSL ages have been recently published in Nian et al., 2018a, 2018b), we constructed a dataset of 344 sediment cores, 658 radiocarbon and 28 OSL ages from the Yangtze Delta. Such a large database is perhaps likely to provide a comprehensive understanding of the Holocene evolution of the Yangtze delta. Our aim is to review the Holocene sedimentary stratigraphic record and the evolution of depositional morphology in an entire deltaic geosystem. This study particularly focuses on the sedimentary discontinuities found in the stratigraphy of many of the sediment cores and discusses the implications for erosional processes linked to morphodynamic adjustments in the Yangtze River mouth during its Holocene history. Sediment trapping rate was then quantified in the delta region on a millennial scale based on the changes in depositional morphology throughout the Holocene to evaluate the present-day degree of sediment starvation. We believe our findings will assist in the understanding of the significant risk of coastal erosion and associated system regime shift induced by intensive human impacts and the predicted acceleration in global sea-level rise for the Yangtze delta. These observations can be applied to other deltas around the world in an uncertain and hazardous future.

2. Regional setting

The Yangtze drainage basin is 1.8×10^6 km^2 in area and has a human population exceeding 400 million. The Yangtze River, longer than 6300 km, discharges 961.6 billion m^3 yr^{-1} freshwater into the East China Sea (ECS). The Asian Monsoon dominates the climate in the drainage basin. The summer monsoon brings precipitation from both the Indian and Pacific Oceans from May to October (the flood season),

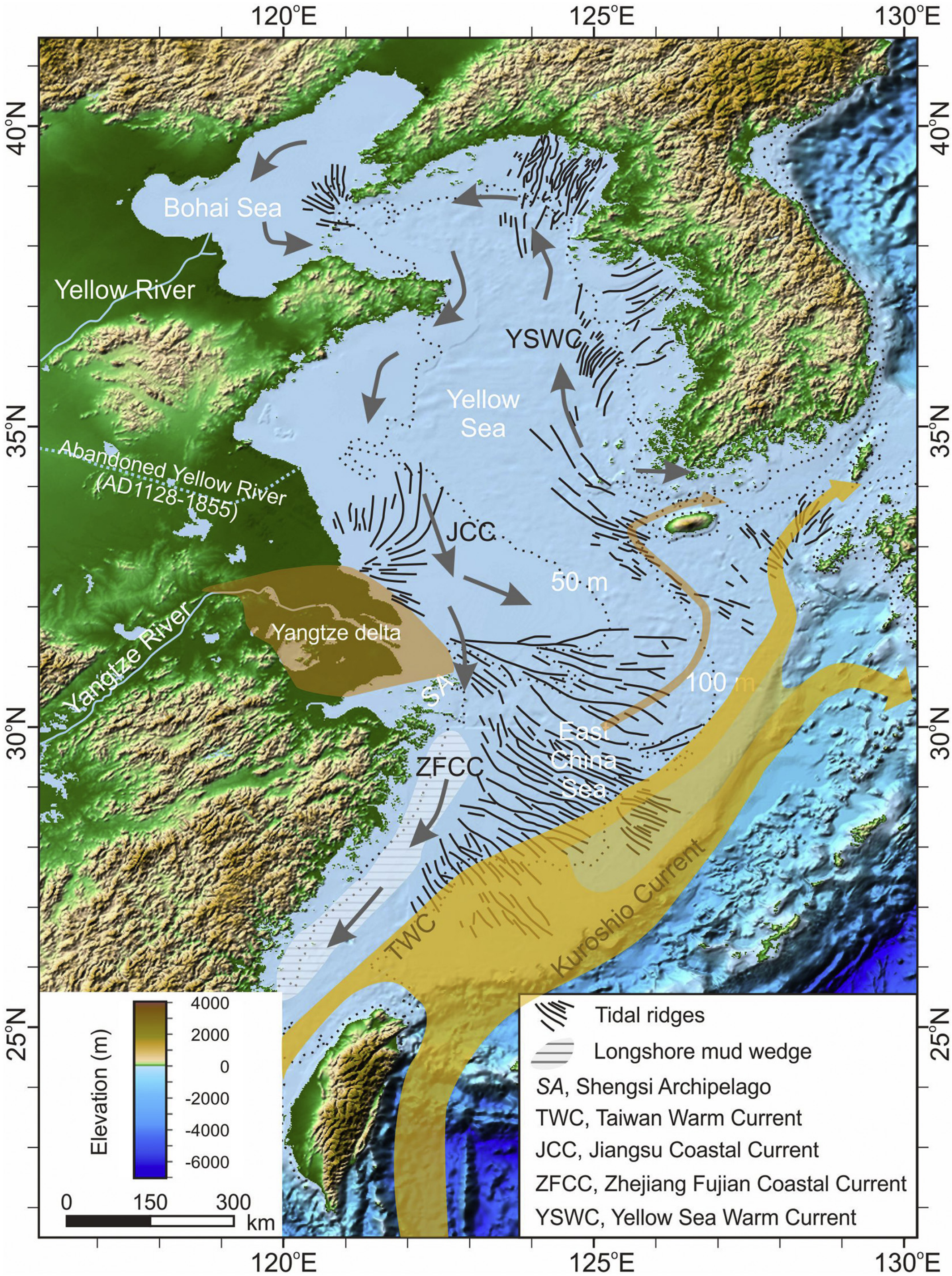

Fig. 3. Ocean and coastal currents in the east China marginal sea (modified after Isobe, 2008; Hsiung and Saito, 2017). Also indicated are the locations of the Yangtze Delta (orange-shaded area), the longshore mud wedge (Liu et al., 2006), tidal ridges on the continental shelf (Li et al., 2014), and locations of the present-day and abandoned (AD1128–1855) Yellow River mouth (Chen et al., 2012). The Taiwan Warm Current and Zhejiang and Fujian Coastal Currents are obvious in summer and winter, respectively (Isobe, 2008). (For interpretation of the references to colour in this figure legend, the reader is referred to the web version of this article.)

which produces 85–98% of the annual sediment load into the ECS (Changjiang Water Resources Commission, 1999). The winter monsoon carries dry and cold air from north and northeast Asia during the dry season. The annual Yangtze sediment load into the river mouth ranged from about 400 to 600 Mt yr^{-1} during the period 1953–1985 (Fig. 2), but very clearly declined to 240–420 Mt yr^{-1} during 1985–2002, owing to dam construction in the drainage basin (Yang et al., 2011). After the impoundment of the TGD in 2003, the annual sediment load declined further because the Reservoir trapped ~180 Mt yr^{-1} sediment in the first decade of its operation (Yang et al., 2014). Since the dam's reservoir was filled to capacity in 2008, the Yangtze sediment load to the sea has remained below 200 Mt yr^{-1} (Fig. 2).

The spatial extent of the Yangtze Delta can be defined as follows. Its apex is recognized at core HG01, which is ~300 km inland from the present-day river mouth (Fig. 1b; Song et al., 2013). Hangzhou Bay borders the southern delta plain (Fig. 1b). The northern boundary of the delta plain was determined using sediment provenance; previous work has discriminated between sediments from the Yangtze and Yellow

Rivers on the basis of their geochemical composition (Yang et al., 2002). In the offshore area, a radiating sand ridge field in the southwest Yellow Sea separates the Yangtze subaqueous delta from the abandoned Yellow River mouth to the north (Figs. 1b, 3; Wang et al., 2012a). The Shengsi Archipelago forms the southern boundary; south of the Archipelago there is a bypass-dominated area that separates prodelta mud from the longshore mud wedge (Fig. 3; Xu et al., 2012).

During the summer season, Yangtze river water disperses eastward and northeastward, driven by the ASM (Beardsley et al., 1985; Chen et al., 1988; Chang and Isobe, 2003). Because it is blocked by the Taiwan Warm Current in the south and east (Fig. 3), most Yangtze suspended sediment is trapped in the inner shelf and added the subaqueous delta. During the winter season, when the East Asian Winter Monsoon (EAWM) prevails, the longshore current resuspends and disperses Yangtze sediment southward, remobilizing material deposited on the subaqueous delta in summer, and depositing a huge longshore mud wedge on the inner shelf of the ECS (Fig. 3; Liu et al., 2006; Xiao et al., 2006). This southward transport of the Yangtze sediment has been estimated to be ~30% of the total suspended sediment load from the River, both in recent decades (Milliman et al., 1985) and throughout the Holocene (Liu et al., 2007).

3. Material and methods

We collected 64 new sediment cores and compiled stratigraphic data from 112 previously published sediment cores from the Yangtze River mouth (Fig. 1b; Table S1). In addition, we used stratigraphic data from 168 cores from the southern Yangtze Delta plain that we had compiled in a previous study (Wang et al., 2012b). Radiocarbon (^{14}C) ages of 345 samples of plant fragments, peat and mollusk shells from the 64 new cores were measured by Beta Analytic using accelerator mass spectrometry (AMS) (Table S2; 36 of which were previously published in Pan et al., 2017; Nian et al., 2018a, 2018b). We also collected 313 ^{14}C ages from the literature (Table S2). All ^{14}C ages were calibrated using the Calib 7.1 program (Stuiver et al., 2015). The Marine13 calibration curve was used for mollusk shell samples. In order to correct for the marine reservoir effect, we used a ΔR value of 71 ± 31, averaged from marine samples from the northwest coast of Taiwan and the Okinawa Trough (Yoneda et al., 2007), for all mollusk shell samples with $\delta^{13}C$ values of 2‰ to −2‰. For shell samples with $\delta^{13}C$ values lower than −2‰, the ΔR value used was −1 ± 143, averaged from samples with similar $\delta^{13}C$ values from Tsingtao, the southwest coast of Korea and the northwest coast of Taiwan (Southon et al., 2002; Kong and Lee, 2005; Yoneda et al., 2007). Reversed ages which we attribute to old carbon (Stanley and Chen, 2000; Wang et al., 2012a, 2012b) were rejected during the chronostratigraphic analysis.

Because material for ^{14}C dating was lacking in sandy sediments, we also measured OSL ages for 28 samples from the newly drilled cores TZ, NT, SD, DY and HA at the State Key Laboratory of Estuarine and Coastal Research, East China Normal University, Shanghai (Table S3). Medium-grained (45–63 μm) and coarse-grained (90–125 μm) quartz was extracted from samples following established procedures (Nian et al., 2015), and was measured for equivalent dose (D_e) using the single-aliquot regeneration dose protocol (Wintle and Murray, 2006). All luminescence measurements were carried out by an automated Risø-TL/OSL DA-20 DASH reader equipped with a $^{90}Sr/^{90}Y$ beta source (Bøtter-Jensen et al., 2003) and an ET EMD-9107 photomultiplier tube. The OSL ages from cores TZ, NT and SD have been reported in our recent geochronology studies (Nian et al., 2018a, 2018b).

Sedimentary facies were identified for these newly obtained sediment cores by comparing the lithology, textures and structures with those reported in previous studies (Fig. 4; Li and Zhang, 1996; Li and Wang, 1998; Hori et al., 2001, 2002b; Wang et al., 2010; Chen et al., 2015; Pan et al., 2017; Yu et al., 2016; Zhang et al., 2017) and observing the distribution of marine microfossils (Table S4). Five delta-wide stratigraphic cross-sections (Figs. 1, 5) were used to assess the architecture, chronology and sedimentary environmental changes throughout the Holocene. We then reconstructed the pre-Holocene basal topography (at 11.7 cal. kyr BP) of the Yangtze River mouth using the stratigraphy of all 344 sediment cores. Furthermore, previous studies point to landmark events in the delta's history: the initiation of Yangtze Delta deposition at 8 cal. kyr BP (Song et al., 2013): summer monsoon weakening and associated reduction in freshwater discharge at 6 and 4 cal. kyr BP (Wang et al., 2005; Zhan et al., 2012), and intensified human activity in the drainage basin (at 2 cal. kyr BP, Wang et al., 2011). This study therefore divides the Holocene history of the Yangtze River mouth into six stages (stage I–VI; 2000 years for each, with the exception of 1700 years for stage I, 11.7–10 cal. kyr BP). Using stratigraphic information, ^{14}C and OSL ages and associated sedimentation rates, we calculated the burial depths (calibrated to present mean sea level; PMSL) at 10, 9, 8, 6, 4 and 2 cal. kyr BP and the thickness of the deposited sediments during each of the six stages in 174 sediment cores (Table S1). Using this large dataset and ArcGis 10.1 software, digital elevation models were constructed for 10, 9, 8, 6, 4 and 2 cal. kyr BP and the total sediment volume was calculated for stages I–VI. Yangtze Delta annual sediment accumulation rates were then calculated for each stage. The sediment mass was obtained by multiplying sediment volume by the dry bulk density, which was measured (based on dry mass of a fixed volume after heating) for 191 samples from onshore cores HM, NT and TZ, and offshore cores HZK6 and HZK9 (Table S5). The dry bulk density was higher for sediments from cores HM, NT and TZ than from cores HZK6 and HZK9, indicating weaker sediment compaction in subaqueous areas. The mean, maximum and minimum values of the dry bulk densities of these five cores were 1.26, 1.71 and 0.87 g cm^{-3}, respectively.

4. Results

4.1. Sedimentological characteristics of major facies

Three depositional systems have been reported for the Yangtze River mouth, fluvial in the last glaciation, estuarine in the early Holocene, and deltaic in the mid- to late Holocene (Li and Zhang, 1996; Li et al., 2000; Hori et al., 2001). The sedimentological characteristics for the major individual facies in these depositional systems have been examined carefully by previous studies (Li and Wang, 1998; Li et al., 2000; Hori et al., 2001; Yu et al., 2016; Zhang et al., 2017). Both Hori et al. (2001) and Zhang et al. (2017) suggested that there was no estuary mouth shoal during the early Holocene. In addition, Zhang et al. (2017) suggested that tidal bar, (terminal) distributary channel, and prodelta mud facies all occurred in a back-stepping deltaic system during the early Holocene, and these can be characterized by abundant foraminifera fossils (Table 1). However, some of our newly drilled sediment cores, SD, HZK2, and HZK8, reveal thick sand bodies at the paleo-river mouth in the early Holocene (Fig. 5). Previous investigation has shown that foraminifera occur only sporadically in the sediments of the turbid deltaic system of Yangtze River mouth (Wang et al., 1988). We therefore conclude that an estuarine depositional system was present in the early Holocene, and we revise the interpretation of individual sedimentary facies, particulary for the paleo-Yangtze estuary based on the schematic diagram by Hori et al. (2001) (Table 1). The sedimentological characteristics for these facies are summarized below.

River channel and paleosol are the two major facies that the post glacial successions rest on in the Yangtze River mouth; river channel facies occurs in the paleo-incised valley and paleosols occur in the paleo-interfluve, i.e., the flanks of the valley (Li and Zhang, 1996; Li et al., 2000). The river channel facies is composed of gravelly sand. Gravel grain diameters vary from a few millimeters to a few centimeters. The sedimentary structure of this facies is always difficult to observe because of disturbance during coring. The paleosol (Chen et al., 2008) facies is characterized by mottled stiff mud with leaching structures and Fe/Mn oxides. OSL dating shows that river channel and

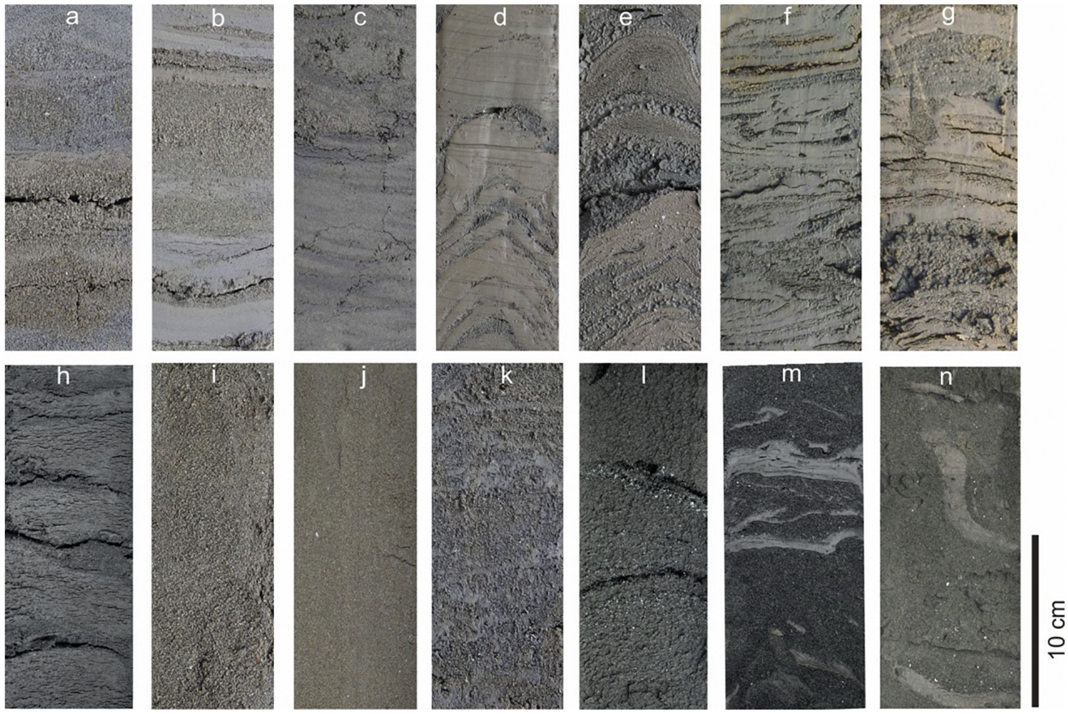

Fig. 4. Photos of typical sedimentary facies. a, tidal river, 60.2–60.4 m in HZK8. b-c, tidal channel, 56.1–56.3 m and 52.4–52.6 m in HZK8. d-e, distributary channel, 2.6–2.6 m and 3.35–3.55 m in HZK1. f-g, muddy tidal flat, 40.6–40.8 m and 41.0–41.2 m in ZK9. h, estuarine front, 42.4–42.6 m in NT. i, estuary mouth shoal, 48.9–49.1 m in HZK8. j, delta front, 7.2–7.4 m in HZK8. k, transgressive lag, 29.8–30.0 m in HZK2. l-n, tidal sand, 45.6–45.8 m in SD, 25.9–26.1 m in HM and 25.0–25.2 m in NT.

paleosol facies were formed during the last glaciation (e.g. the gravelly sediment deposition at the base of core SD was dated to 62 ± 6 kyr BP, Fig. 5b; Table S4; Zhao et al., 2008; Wang et al., 2013; Nian et al., 2018b).

Tidal river facies (tide-influenced fluvial channel in Zhang et al., 2017) mainly consists of a fining-upward succession of fine to coarse sand. The sand is commonly intercalated with thin mud layers and mud clasts (Fig. 4a; Pan et al., 2017). Foraminifera are sporadically present (Fig. 5).

Tidal channels (distributary channel in Hori et al., 2001 and tidal-channel-floor in Zhang et al., 2017). This facies is characterized by sand-mud couplets. Sand and mud layers are interbedded (thickness of single sand layer > 1 cm) in the ebb-dominated channel, and are interlaminated (thickness of single sand layer < 1 cm) in the flood-dominated channel (flood barb) (Fig. 4b, c; Hori et al., 2001). The distributary channel facies (Fig. 4d, e) in the deltaic system (Table 1) has features similar to the tidal channel in the estuarine system. In addition, Li et al. (2009) described a tide-influenced inlet fill facies (simplified as tidal inlet fill in this paper). The sedimentary structures and succession of tidal inlet fill facies is similar to that of the ebb-dominated tidal channel.

Muddy intertidal to subtidal flat facies (Fig. 4f, g; Hori et al., 2001; Wang et al., 2010; Pan et al., 2017) is present in both estuarine and deltaic systems. A succession of sand-mud couplets with vertically changing thicknesses of single layers characterizes the sequence of intertidal to subtidal flat (Li and Wang, 1998). Sharp boundaries between single sand and mud layers is the major feature of the sand-mud couplets of the tidal flat facies (Hori et al., 2001). Mud predominates in the upper tidal flat with minor silt or sand layers. Both the thickness and frequency of sand layers increase in the middle and lower tidal flat. Sand predominates in the lower and subtidal flat with some mud layers present.

Estuary front (distal muddy deposits at the mouth of a tide-dominated system in Zhang et al., 2017). This facies is characterized by a high mud content. Thin layers and lenses of sand (Fig. 4h) occur in a fining-upward succession. The prodelta-shelf facies in the deltaic system is also mud-dominated with some silt or sand laminations and lenticular bodies. This facies is characterized by a coarsening-upward succession and is always underlain by the fining-upward succession of the estuarine front facies with a transitional boundary.

The estuary mouth shoal and delta front facies are both composed of structureless sands (Fig. 4i, j) and overlain by intertidal sediments. But the estuary mouth shoal sand is coarser (Pan et al., 2017; Fig. 4i, j) and contains a higher abundance of marine microfossils (cf. core ECS0702, Liu et al., 2010).

Tansgressive lag. This facies is characterized by mixture of sand, mud, abundant shell fragments and heavy biogenetic disturbance (Fig. 4k).

Tidal sand (ridge). In addition to the three depositional systems mentioned above, there is a tidal sand ridge field in the south Yellow Sea adjacent to the present-day Yangtze River mouth (Fig. 3; Wang et al., 2012a). Hori et al. (2001) recognized the tidal sand ridge facies in core JS98 and Hori et al. (2002b) proposed that there was a tidal sand ridge field in the northeast part of the paleo-Yangtze River mouth after ~8000 ^{14}C years BP (uncalibrated age). We recognized tidal sand (ridge) facies in several newly drilled sediment cores (NT, HM, SD, and DY). This facies is characterized by a fining-upward succession and a sharp contact with the underlying mud layer. Thick layers of sand occur in the lower section, intercalated frequently with mud intraclasts and thin layers of mud, plant fragments, and micas (Fig. 4l–n). The thickness of the sand layers decrease upward and mud dominates the upper section. There is always more than one fining-upward succession in the tidal sand sequence.

4.2. Late Quaternary stratigraphic architecture across the Yangtze River mouth

Five age-constrained stratigraphic cross-sections reveal the stratigraphic architecture across the Yangtze Delta (Fig. 5). The stacking of stratigraphic successions, chronological relationships, interpretation of

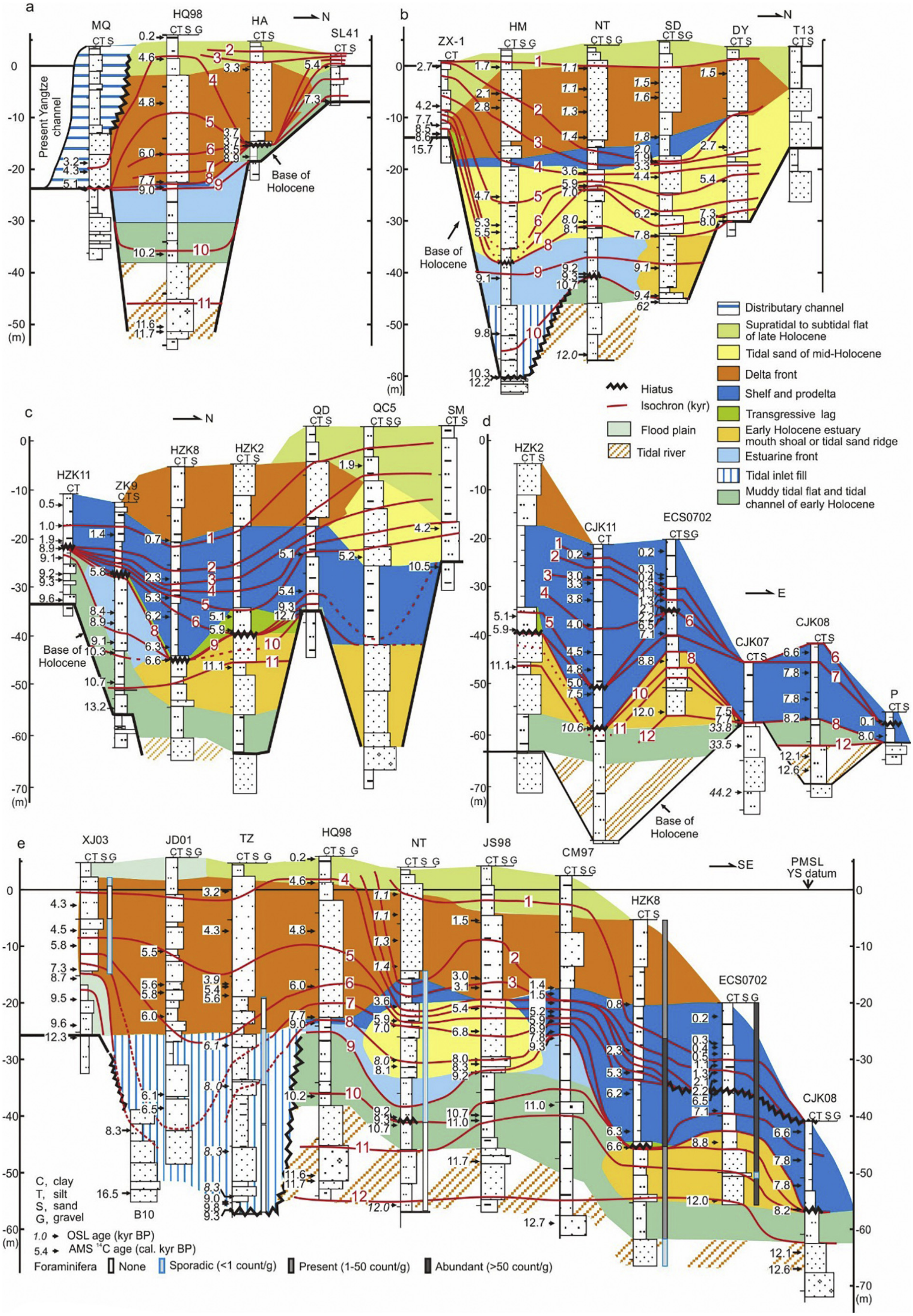

Fig. 5. Stratigraphic cross-sections with isochrons of the Yangtze Delta, including detailed information about the lithology, dating, and sedimentary facies. a–c) Transverse cross-sections. d) Offshore cross-section. e) Longitudinal cross-section. Abundance of foraminifera along this section is also indicated. Note only the lower section of core B10 is presented to show the sedimentation before 8.3 cal. kyr BP to compensate the lack of strata in the nearby core JD01 (Fig. 1b; Li et al., 2009). Data source of sediment cores and chronology are indicated in Tables S1 and S2.

Table 1
A comparison of sedimentary facies descriptions in the paleo-incised Yangtze valley. These facies are grouped into three depositional systems: deltaic, estuarine, and fluvial in descending order. The boundary between deltaic and estuarine system was not distinguished in Li et al. (2000). The estuarine system was proposed to be a back-stepping delta in Zhang et al. (2017). The estuary mouth shoal facies was newly introduced in this study.

This study	Li et al., 2000	Hori et al., 2001	Zhang et al., 2017
Delta plain (supratidal to subtidal flat and distributary channel)	Deltaic	Intertidal to subtidal flat	Not discussed
Delta front		Delta front	
Prodelta-shelf	Estuary-shallow	Prodelta	
Tidal sand (ridge)	marine	Tidal sand ridge	
Transgressive lag			
Estuary		Estuary	Back-stepping delta
Estuary mouth shoal, tidal ridge		Not found, tidal ridge suggested	Tidal-bar or distal muddy deposits (prodelta mud) at the mouth of a tide-dominated system, (terminal) distributary channel
Estuary front		Estuary front	
Muddy intertidal to subtidal flat	Floodplain-estuary	Muddy intertidal to subtidal flat	Not reported
Tidal channel (Tidal inlet fill)		Distributary channel	Tidal-channel-floor
Tidal river		Tidal river	Tide-influenced fluvial channel
River channel	River channel	Fluvial	Amalgamated Fluvial Channel

sequence stratigraphy, and the sedimentary evolution of each cross-section are described below.

MQ–HQ98–HA–SL41 in the upper delta plain (Fig. 5a). Core HQ98 is located in the paleo-incised Yangtze valley and has a pre-Holocene basal depth of about −50 m. The other three cores are on the south and north flanks of the paleo-valley, and their bases are in late Pleistocene paleosol facies at depths between −24 and −18.5 m. In core HQ98, successions of tidal river, muddy tidal flat, and estuary front occur from about 12 to 9 cal. kyr BP from the core bottom upwards, overlaid by prodelta, delta front and tidal flat successions that formed over past 9000 years (Hori et al., 2001). On the northern flank, tidal flat facies appear above the paleosol in core HA, dated at 8.9–8.5 cal. kyr BP. This tidal flat succession is topped by an erosional surface characterized by layers of mud intraclasts (Fig. 6a). Deltaic sand facies, dated to 3.7–3.0 cal. kyr BP sit above the erosional surface at this site. The tidal flat succession constitues the whole Holocene sequence, which is dated back to 7.3 cal. kyr BP in core SL41. In core MQ on the southern flank, a series of delta front sands, dated to 5.1–3.2 cal. kyr BP, occur immediately above the paleosol, overlain by muddy distributary channel deposits.

Therefore, a very typical Holocene stratigraphic sequence, i.e., the transgressive systems tract (TST) of an estuarine sequence and the highstand systems tract (HST) of the deltaic sequence occurs in the paleo-incised valley along this cross-section. In contrast, long periods of sedimentary hiatus characterize the boundary between the HST of deltaic or tidal flat sequences and the paleosol or TST of tidal flat sequences on the southern and northern flanks. Dating results show that in the HST, the sandy shoal at the river mouth was first deposited in the paleo-incised valley (HQ98) ~8000 years ago, followed by vertical accumulation for > 3000 years. This sand body then expanded southward beginning at ~5000 years ago and northward after ~3700 cal. yr BP.

ZX-1–HM–NT–SD–DY–T13 in the middle delta plain (Fig. 5b). The stratigraphy is much more complicated along this cross-section, except in ZX-1, which consists of a simple tidal flat sequence deposited after 8.6 cal. kyr BP above the late Pleistocene paleosol. Riverbed gravelly sands from the late Pleistocene occur in HM, NT, and SD, which are located within the paleo-incised valley. Above the riverbed sands in HM, a 20-cm thick layer of mud and gravels appears; it is then overlain by a succession of tidal inlet fill with a sharp basal contact. Large mud intraclasts containing plant fragments occur on the contact (Fig. 6b). A radiocarbon age of ~12.2 cal. kyr BP was obtained from the mud-and-gravel layer and another radiocarbon age of ~10.3 cal. kyr BP was obtained from the plants in the mud intraclasts (Fig. 5b). This facies sequence and dating results indicate that an incision of the tidal inlet occurred at site HM after 10.3 cal. kyr BP. The tidal inlet fill succession is characterized by thickly interbedded sand and mud and was dated at ~9.8 cal. kyr BP (Fig. 5b). The estuarine front succession, ~9.1 cal. kyr BP, then overlies the tidal inlet fill.

In contrast, tidal river and tidal flat successions, with ages of 12 kyr (OSL age, years prior to 2014 when samples were collected) to 10.7 cal. kyr BP appear at the bottom of the Holocene sequence in NT, overlain by estuarine front facies dated at 9.2 cal. kyr BP with an erosional contact. A 20-cm thick layer of calcareous nodules mixed with abundant shell fragments (Fig. 6c) characterizes this erosional contact, and dating results below and within this layer indicate a depositional hiatus between 10.7 and 9.2 cal. kyr BP. In SD, a thick tidal sand succession, 9.4–7.8 cal. kyr BP in age, occurs above the riverbed gravelly sand (Fig. 5b).

Stacking of tidal sand and deltaic successions then occurs in all cores except ZX-1, above the lower estuarine front, tidal sand or paleosol facies. A sharp contact occurs at the bottom of this sequence in HM, although muddy sediments prevail both below and above the contact (Fig. 6d). Dating resuts further indicate a uniform chronology, i.e., ~8.0 cal. kyr BP of the base of this sequence in all cores (Fig. 5b). Therefore, we interpret the stacking of tidal inlet fill and estuarine front in HM, tidal river, tidal flat and estuarine front in NT, and tidal sand in SD as constituting the TST in the paleo-incised valley. We also conclude that the series of tidal sand and deltaic facies represents the HST in all cores.

Furthermore, the stratigraphic architecture of HST tidal sand along this cross-section is informative for its temporal and spatial evolution. The chronostratigraphy and sedimentary architecture indicate that tidal sand was first deposited at NT, SD and DY, while erosion or sedimentary hiatus occurred at the HM location at ~8.0 cal. kyr BP (Fig. 5b). The locus of high sedimentation rates then migrated rapidly among these cores during 8 to 5 cal. kyr BP. For example, rapid deposition took place at HM, while accretion slowed significantly at NT at ~7–6 cal. kyr BP. Sharp contacts occur frequently in these successions (Fig. 6e). A tidal ridge-and-trough depositional system can therefore be inferred from 8 to 5 cal. kyr BP. Tidal sheet sands then prevailed as the troughs were mostly infilled after ~5 cal. kyr BP and deposition ceased in the cores from south to north in a temporal sequence from 4 to 2 cal. kyr BP.

HZK11–ZK9–HZK8–HZK2–QD–QC5–SM in the lower delta plain and subaqueous delta (Fig. 5c). Stratigraphic architecture demonstrates that riverbed or tidal river deposition occurred at the bottom of three cores, HZK8, HZK2, and QC5, while the other cores have paleosols at their bases. This transect therefore reveals two paleo-incised sub-valleys, separated by a terrace where core QD is located.

Thick sandy successions of estuary mouth shoal occur in HZK2 and HZK8, overlying muddy tidal flat facies or channel deposits. There are transgressive lags on the top of the shoal successions with sharp contacts in both HZK2 and HZK8 (Fig. 6f, g). A coarsening-upward

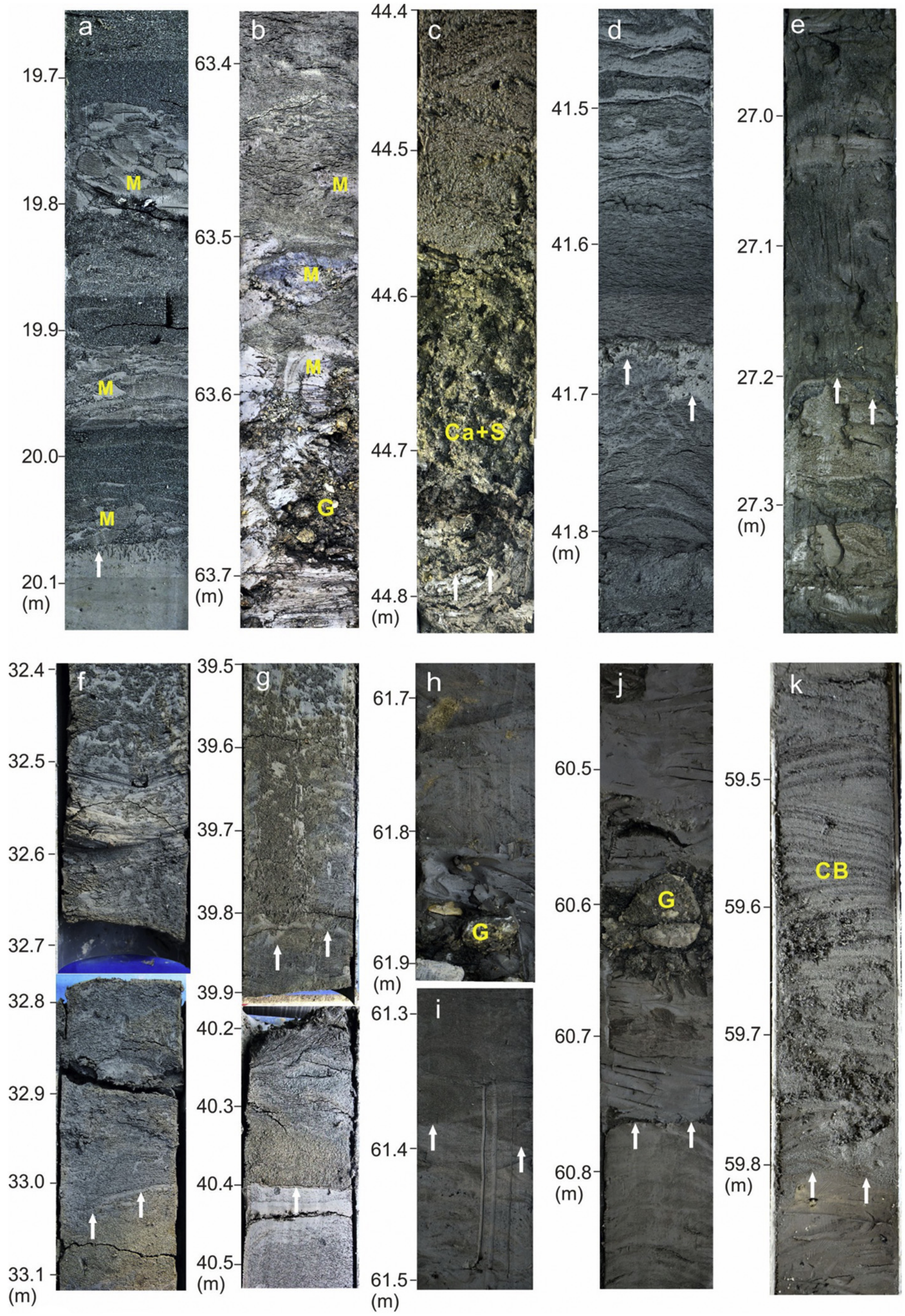

Fig. 6. Major erosional or sharp contacts in different cores with core depth indicated to left. The white arrow denotes erosional or sharp contact. M, mud intraclasts; G, gravel; Ca, calcareous nodule; S, shell fragments; CB, cross bedding. a, core HA; b and d, core HM; c and e, core NT; f, core HZK2; g, core HZK8; h–k, core TZ.

sequence from shelf-prodelta to delta front deposits appears above the transgressive lag (Fig. 5c). Thus, the TST is made up of a stack of tidal river, flat and channel and estuary mouth shoal deposits in HZK2 and HZK8. Radiocarbon ages obtained from these cores and a comparison with other cores suggest that the mouth shoal was formed before 10 cal. kyr BP (Fig. 5c), when the tidal river and muddy flat deposits developed in the two cross-sections described above (Fig. 5a, b). The transgressive lag was dated at 6.6–5.1 cal. kyr BP (Fig. 5c), indicating a long period of no sedimentation on the shoal after ~10 cal. kyr BP. Deposition of the HST occurred mainly after ~6 cal. kyr BP. The stratigraphy in QC5 (Zheng, 1989) is similar to that in HZK2 and HZK8. One major difference is that there is a fining-upward sandy succession formed from 5.2 to 1.9 cal. kyr BP, possibly a tidal sand deposit like those in cores SD, DY (Fig. 5b) and in core SM (Wang et al., 2012a, 2012b).

In core QD, a thin layer of tidal flat deposits occurs above the basal paleosol, overlain by deltaic successions formed after ~5.4 cal. kyr BP. In core ZK9, successions of tidal flat and estuarine front deposits occur above the paleosol. A thin layer of transgressive lag overlies the estuarine front deposits and it is then overlain by shelf and prodelta mud (Wang et al., 2010). Dating results demonstrate that the HST of shelf and prodelta mud was formed around 5.8 cal. kyr BP and after, and the estuary TST deposits were formed before ~8 cal. kyr BP (Wang et al., 2010); which would indicate a sedimentary hiatus from 8 to 6 cal. kyr BP. In core HZK11 on the southern flank of the paleo-valley, tidal flat successions occur above the paleosol and they are overlain by shelf mud with a sharp contact. Radiocarbon ages indicate that the tidal flat sediments accumulated mainly during 9.6 to 8.9 cal. kyr BP and shelf mud was deposited after 1.9 cal. kyr BP (Fig. 5c), reflecting a long sedimentary hiatus beginning at ~8.9 cal. kyr BP.

HZK2–CJK11–ECS0702–CJK07–CJK08–P in the subaqueous delta (Fig. 5d). Successions of tidal river, flat, and estuary mouth shoal are stacked in the lower section of the post glacial stratigraphy in these cores; shelf and prodelta mud dominates the upper section. In some core locations, such as at CJK11, shelf mud was deposited after ~8 cal. kyr BP, and it directly overlies tidal flat deposits formed before 10.6 kyr. Such architecture indicates that a ridge-and-trough system was present before 8 cal. kyr BP, with ridges occurring at the site where the estuary mouth shoal had developed (such as HZK2 and ECS0702) and troughs developed at sites away from the mouth shoal. Dating results show that the sedimentation of shelf and prodelta mud occurred in all cores during the ~8 to 6 cal. kyr BP period. After that, shelf and prodelta mud deposition ceased; it then resumed in the cores at different times: after ~5 cal. kyr BP in the nearshore cores HZK2 and CJK11, at ~2.2 cal. kyr BP in the seaward core ECS0702, and only < 200 years ago in the distal core P (Fig. 5d). This chronostratigraphic trend indicates a significant landward retreat of the depositional system at ~6 cal. kyr BP, with obvious seaward progradation only occurring over the past 2000 years.

XJ03–JD01 (B10)–TZ–HQ98–NT–JS98–CM97–HZK8– ECS0702–CJK08 from the delta apex to distal mud (Fig. 5e). There are five types of Holocene stratigraphic architecture in the paleo-incised valley along this longitudinal profile. The first type, represented by JD01 and TZ at the apex of the delta, is constituted by a succession of tidal inlet fill in the lower section and deltaic deposits in the upper section of the Holocene stratigraphic sequence. The second type of Holocene stratigraphic sequence consists of tidal river, channel/flat, estuarine front successions of the TST, and prodelta, delta front and delta plain successions of the HST, as reported from cores HQ98 and CM97 in previous studies (cf. Hori et al., 2001). Thirdly, there are tidal sand deposits occurring between the deltaic and estuarine sequences such as in cores NT and JS98. The fourth type, seen in nearshore cores HZK8 and ECS0702, is characterized by successions of the estuary mouth shoal in the upper portion of the estuarine sequence. The last type occurs in offshore core CJK08, where tidal river, flat and shelf or prodelta mud facies make up the entire Holocene sequence.

Most features of the five types of stratigraphic architecture have been described in the above cross-sections. Here we focus only on the first type, characterized by thick accumulations (~30 m) of tidal inlet fill. At the bottom of the Holocene sequence in TZ, brownish-gray silty mud, ~0.5-m thick, abruptly overlies river channel gravels (Fig. 6h). A radiocarbon age of 9.3 cal. kyr BP was obtained from plant fragments in this mud layer. The mud is then overlain by ~0.6-m of silt and clayey silt with a sharp contact (Fig. 6i). Further upward, a 0.9-m thick layer of homogeneous mud is intercalated with a gravel layer (7-cm thick) in the lower part of the section (Fig. 6j), and two radiocarbon ages obtained from plant fragments from the top of this section have ages of 9.8 and 9.0 cal. kyr BP (Fig. 5). This succession of muddy sediments (~2 m total thickness, with an age of 9.8 to 9.0 cal. kyr BP) contains no marine microfossils (Table S4), indicating that it was deposited in a freshwater environment, most likely the floodplain. However, such an inference conflicts with paleo-sea level estimates of ~ −35 to −25 m at that time (Bard et al., 1996), because this floodplain succession appears at a depth of −57 to −55 m. Based on the evidence of the reversed ages and frequent abrupt contacts within the succession, we suggest that these deposits were bank slides delivered to the floor of the tidal inlet owing to lateral erosion after 9.3 cal. kyr BP.

Above the muddy bank slide deposits and with an erosional contact, there is a 40-cm thick layer of fine sand with clear cross bedding (Fig. 6k), additional evidence for strong currents in the tidal inlet. After this, sand and mud layers are interbedded with weak boundries between beds. These occur for ~30 m and are dated to 8.3 to 6.0 kyr BP (Nian et al., 2018a; Table S3), indicating rapid infilling of the tidal trough. In a similar manner, the tidal inlet fill of core JD01 was deposited primarily during 7 to 6 cal. kyr BP (Li et al., 2009). Therefore, at the apex of the Delta, the Holocene sequence formed after ~8.3 cal. kyr BP, while erosion dominated in earlier period.

4.3. Major types of sedimentary discontinuities

Researchers have known about the sedimentary discontinuities in the late Quaternary stratigraphy of the Yangtze River mouth for a long time (Li and Zhang, 1996). Taking advantage of our newly drilled sediment cores which preserve many erosional or sharp contacts (Fig. 6), we are able to group these discontinuities into two major types according to their relationship to the sedimentary successions. Radiocarbon and OSL dating results obtained in close proximity to these contacts further deepened our understanding of these discontinuities.

The first type reflects significant erosion at the bottom of tidal inlet fill successions and on the top of tidal flat successions during the early Holocene. This includes the erosion observed in the lower section of core TZ, dated 9.3–8.3 cal. kyr BP in the upper delta plain (Figs. 5e, 6h–k) and in the lower portion of core HM after 10.3 cal. kyr BP in the middle delta plain (Figs. 5b, 6b). Comparison of sedimentary facies and chronology with adjacent sediment cores suggests that two tidal troughs about 30 m and 20 m deep occurred at TZ and HM, respectively, during the periods of erosion (Fig. 5b, e). Erosion was also observed on top of the early Holocene tidal flat successions at NT from ~10.7 to 9.2 cal. kyr BP, after 8.9 cal. kyr BP at core HZK11, and after 8.5 cal. kyr BP at core HA (Fig. 5a–c; Fig. 6a, c). Thus, the erosion process started in the paleo-incised valley, expanded to include the southern and northern flanks and then migrated landward in a temporal sequence from 10.7 to 8.3 cal. kyr BP, with the most significant and widespread erosion occuring between 9.3 and 8.3 cal. kyr BP.

The second type of sedimentary discontinuity was observed at the top of tidal ridge or the bottom of tidal trough successions in early to mid-Holocene age sediments. The sharp boundaries between the estuary mouth shoal successions and transgressive lag successions in cores HZK2 and HZK8 (Fig. 6f–g), together with their chronology (Fig. 5c), indicate that a long depositional hiatus occurred on the top of the estuary mouth shoal. A chronostratigraphic comparison along our cross-sections further suggests that a tidal ridge-and-trough (~15–20 m relief) system was formed after ~10 cal. kyr BP and sedimentation only occurred on the ridges after ~6–5 cal. kyr BP (Fig. 5c, d).

Another ridge-and-trough system was present during the mid-Holocene, located in the present-day middle delta plain (Fig. 5b). Radiocarbon ages below and above the sharp contacts of the tidal trough sediments in core HM (Fig. 6d) indicate a long interval of erosion in the trough starting at ~9 cal. kyr BP (Fig. 5b). This ridge-and-trough system stopped further development after ~6 cal. kyr BP as accretion of the ridge slowed significantly (Fig. 5b). These sediments were overlain by successions of tidal sheet sand above an abrupt boundary, as can be seen in core NT (Fig. 6e). Significant reworking of sediments on the top of the tidal ridge after ~ 6 cal. kyr BP can be inferred from the frequent occurrence of mud intraclasts in sheet sands (Fig. 4n).

Additionally, sedimentary hiatuses were inferred, based on lithology and chronology, in shelf-prodelta successions after ~6 cal. kyr BP, such as in cores ECS0702, CJK07, CJK08 and P (Fig. 5e; Liu et al., 2010). Sediment accumulation returned to the shelf ~2000 years ago in ECS0702, while other cores, such as CJK07, CJK08 and P have seen little depositon in the late Holocene/modern (Fig. 5d, e).

4.4. Summary of sequence stratigraphy in the Yangtze River mouth

The spatial distribution of sequence stratigraphy (Fig. 7) is complex in the Yangtze River mouth. Typical transgressive and regressive successions reported by previous studies (cf. Van Wagoner et al., 1988; Posamentier and Allen, 1999; Dalrymple and Choi, 2007) have been found at some locations associated with the river mouth. However, the maximum flooding surface (MFS) is difficult to recognize in most

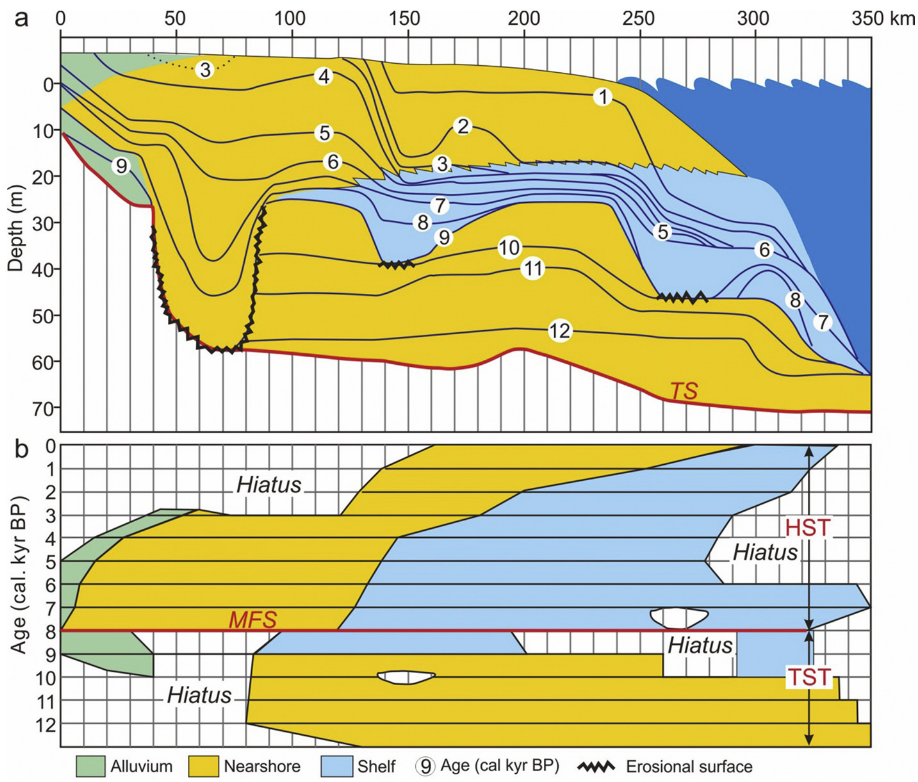

Fig. 7. Summary of the Holocene sequence stratigraphy across the Yangtze River mouth. (a) Chronostratigraphic chart. Blue lines represent the chronostratigraphic surfaces. (b) Wheeler diagram. Abbreviation: MFS, Maximum flooding surface; TS, transgressive surface; HST, highstand systems tract; TST, transgressive systems tract. (For interpretation of the references to colour in this figure legend, the reader is referred to the web version of this article.)

locations because there are many sedimentary discontinuities and disturbances caused by thick successions of tidal inlet fill and tidal ridge-and-trough system sediments (Fig. 5). The fact that the TST was mostly absent in cores at the head of the paleo-incised valley (such at at JD01 and TZ, Fig. 7a) was also difficult to document without careful observation of the trough-floor depositional styles and the help of a detailed chronology. This is because the sedimentary structure of tidal inlet fill successions (Li et al., 2009) is very similar to that of tidal channel facies in a tide-dominated estuarine setting (Hori et al., 2001); both are characterized by interbedded sand and mud layers with weak boundaries. By observing the depositional system across the entire river mouth, we found that it retreated landward at a slow rate before 10 cal. kyr BP, and the retreat accelerated significantly during the 10 to 8 cal. kyr BP period, except for some isolated deposition on the shelf (identified as mud ridges; Fig. 5d; Feng et al., 2017). After this (8 to 6 cal. kyr BP), the locus of deposition moved > 100 km seaward. We therefore suggest that the MFS occurred at ~8 cal. kyr BP as delta sedimentation began at the the apex of the estuary system at that time (Song et al., 2013). Significant retreat of shelf deposition was seen again after 6 cal. kyr BP and progradational shelf clinoform are present after 5 cal. kyr BP. It is thus easy to misidentify the retreating surface at 6 cal. kyr BP as the MFS in the offshore area.

4.5. Millennial-scale morphological evolution during the Holocene

In our paleo-topographic reconstruction based on dated sedimentary cores (Tables S1, S2) the pre-Holocene basement of the paleo-incised Yangtze valley is narrow and deep, outlined by the sharp gradient of the −60 to 0 m contours (relative to the PMSL) in the upper valley. The lower part of the valley is wider and shallow as outlined by the −60 to −30 m contours (Fig. 8a). There is a major terrace (topped by a late Pleistocene paleosol) buried at ~−25 m depth within the upper valley, and a minor terrace at ~−35 m depth within the lower valley. These buried paleosols, between −20 and −40 m depth, are wide and flat on both the northern and southern flanks of the valley, and they represent terraces formed during the last glaciation, prior to 20,000 years ago (Wang et al., 2012b).

The topography of the pre-Holocene basement controlled the shape of the river mouth in association with sea-level rise from the early to mid-Holocene. A long and narrow inner estuary and a broad outer estuary were formed when sea level rose to ~−35 m at 10 cal. kyr BP (Bard et al., 1996; Lambeck et al., 2014), two regions that were separated by a large mouth shoal that developed on the base of the minor terrace (Fig. 8b). There was a small scoured trough (the tidal inlet; extending below −50 m) upstream of the river mouth shoal at that time. As sea-level rose the mouth shoal and terraces in the valley and on the southern and northern flanks were gradually submerged, which led to a funnel-shaped river mouth at 9 cal. kyr BP (Fig. 8c). A significant tidal inlet sitting ~40–60 m below PMSL appeared in the upstream portion of the terrace in the upper valley at 9 cal. kyr BP. The river mouth shape at 8 cal. kyr BP was similar to that at 9 cal. kyr BP except that the former outer estuary was submerged (Fig. 8d). Ridge and trough morphology developed in the offshore subaqueous valley, indicating a tide-dominated environment in the valley at that time (Feng et al., 2017).

The river mouth remained funnel-shaped at 6 cal. kyr BP, when the sea had risen to close to the present-day level (Fig. 8e). The former tidal inlet in the upper valley was mostly infilled at that time. Ridge morphology was still present in the offshore valley. By 4 cal. kyr BP, the tidal inlet had filled in completely, and a delta-front platform had appeared at the river mouth (Fig. 8f). By 2 cal. kyr BP, a delta plain had formed in the upper valley, with distributaries and elongated river mouth bars constituting deposition on the majority of the delta front platform (Fig. 8g). The coastline moved little on the southern and northern delta plains between 6 and 4 cal. kyr BP and clearly prograded seaward after 4 cal. kyr BP.

4.6. Sediment trapping rate in the Holocene and recent history

The millennial scale sediment accumulation volume was calculated using the digital elevation models of the paleo-topography (Fig. 8) described above, and this was converted to sediment mass (Table 2)

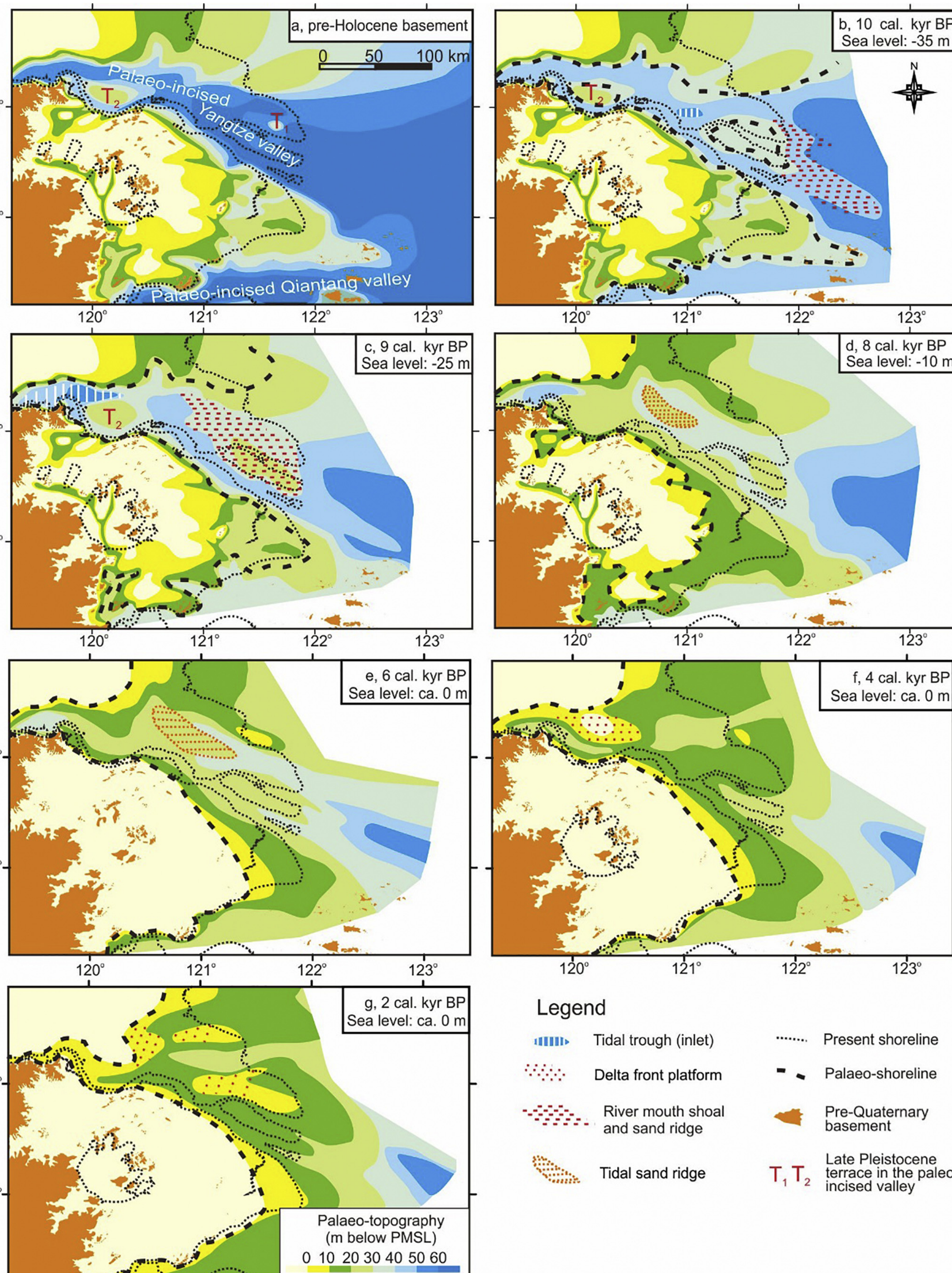

Fig. 8. Morphological changes in the Yangtze River mouth, reconstructed based on the chronostratigraphy and the dataset in Table S1. (a) pre-Holocene basal topography; (b) 10 cal. kyr BP; (c) 9 cal. kyr BP; (d) 8 cal. kyr BP; (e) 6 cal. kyr BP; (f) 4 cal. kyr BP; and (g) 2 cal. kyr BP. Sea levels are from Bard et al. (1996), Lambeck et al. (2014), and Wang et al. (2013).

Table 2
Millennial scale sediment budget of the Yangtze coast calculated from the topographic changes as shown in Fig. 8 and annual sediment accumulation in the very recent history. Total sediment volumes in stages VII and VIII are collected from Li et al. (2011); those in stages IX and X are from Li et al. (2015). Annual sediment mass was calculated on the basis of the mean (1.26 g cm^{-3}), maximum (1.71 g cm^{-3}) and minimum (0.87 g cm^{-3}) sediment dry bulk density in cores HM, NT, TZ, HZK6 and HZK9 for stages I–VI. For stages VII–X, the mean (1.12 g cm^{-3}), maximum (1.47 g cm^{-3}) and minimum (0.87 g cm^{-3}) values of the dry bulk density were calculated from the top 10-m of sediment in cores HZK6 and HZK9, which were obtained from the subaqueous delta. Negative values in stage X indicate net erosion.

Stage	Time period (cal. kyr BP/AD)	Total volume of deposited sediment	Volume of sediment deposited annually	Annual sediment mass (10^6 t yr^{-1})		
		(10^9 m^3)	(10^6 m^3 yr^{-1})	Avg.	Max.	Min.
I	11.7–10	300.95	150.5	224	302	154
II	10–8	217.29	108.7	137	186	95
III	8–6	239.09	119.6	151	205	104
IV	6–4	156.55	78.3	99	134	68
V	4–2	179.56	89.8	113	154	78
VI	2–0	256.75	128.9	162	220	112
Average value in stages I–VI		225.03	112.6	148	193	98
VII	1958–1979	3.97	189.2	212	278	165
VIII	1979–2002	1.92	83.3	93	122	72
IX	2002–2011	0.40	43.9	49	65	38
X	2011–2013	−1.14	−570.0	−638	−838	−496

Note: 0 cal. kyr BP = CE 1950.

using the dry bulk density of the sediments (Table S5). Sediment deposition amounts were divided into six stages (I–VI; Fig. 9), each lasting 2000 years (except for a 1700 year-long stage I). The largest annual sediment mass deposited in the river mouth occurred in stage I, when deposition averaged 224 Mt dry weight yr^{-1} (Table 2). The annual sediment mass then decreased significantly to 137 Mt yr^{-1} (a 61% decrease) during stage II (10–8 cal. kyr BP), despite the strongest summer monsoon at that time (Fig. 9b). High trapping rates were also calculated for 8–6 cal. kyr BP (151 Mt yr^{-1}, ~67% of that in stage I) and 2–0 cal. kyr BP (162 Mt yr^{-1}, ~72% of that in stage I); the earlier is consistent with the strong summer monsoon (Fig. 9b) and a decelerated sea-level rise (Fig. 9e), and the latter corresponds with intensified human activity in the drainage basin (Fig. 9d). In contrast, trapping rates were low between 6 and 2 cal. kyr BP (99–113 Mt yr^{-1}, ~44–50% of that in stage I) during a period of a weaker summer monsoon after ~6 cal. kyr BP (Fig. 9b), a stronger winter monsoon at ~4–3 cal. kyr BP (Fig. 9c) and low levels of human impact on sediment yield (Fig. 9d).

We also define four additional stages, VII to X, to encompass the very recent history of the delta (ca. 60 years; Table 2), during which sediment volumes were reported in previous studies based on marine charts and measurement of subaqueous topography (Li et al., 2011; Li et al., 2015). We calculated the annual sediment mass according to these reports, and compare these with Holocene deposition. Stage VII reflects a high sediment trapping rate (212 Mt yr^{-1}) corresponding to high sediment loads from the 1950s to the 1970s (Fig. 2); Stage VIII is the interval of low trapping rate (93 Mt yr^{-1}) between 1979 and 2002 which is after the peak in regional deforestation (Lu and Higgitt, 1998) and before completion of the Three Gorges Dam (TGD). Stage IX is an interval of lower trapping rate after completion of the TGD in 2003 (49 Mt yr^{-1}, only ~22% of the trapping rate in stage I; Fig. 9a). Finally, in stage X, this region has seen net erosion after 2011. Therefore, the sediment trapping rate in the river mouth has been substantially lower than values measured during the Holocene since the construction of the TGD (Table 2).

5. Discussion

5.1. Morphodynamic response of the river mouth to sea-level rise during early Holocene

Based on the late Quaternary stratigraphic architecture and major types of sedimentary discontinuities, it can be seen that significant erosion occurred in the tidal river, on the tidal flat within the estuary, and in the offshore tidal trough, accompanied by a rapid landward retreat of the river mouth depositional system between 10 and 8 cal. kyr BP (Figs. 5–7). The reconstructed paleo-topographic map (Fig. 8) and associated sediment budget (Table 2; Fig. 9a) further reveals a significant decline in sediment trapping rate in the paleo-Yangtze estuary, which is in agreement with the stratigraphic records of an erosion dominated state during this period. We suggest that the Yangtze estuary changed from a constructive phase into a destructive phase, which was induced by the combined effect of two factors, rapid sea-level rise and associated change in river mouth shape from sheltered and elongated before 10 cal. kyr BP to open and funnel-shaped thereafter (Figs. 8b–d, 10).

The first factor, rapid sea-level rise not only provided extra accommodation space, but also strengthened marine processes in the river mouth during the 10 to 8 cal. kyr BP period. Sea-level rise was slow early in stage I (~2 mm yr^{-1}) and then accelerated after ~11.5 cal. kyr BP and reached a rate of ~10–11 mm yr^{-1} during 11.1–10 cal. kyr BP (Lambeck et al., 2014; Fig. 9e). In contrast, the rate of sea-level rise exceeded 10 mm yr^{-1} during the most time of stage II (Lambeck et al., 2014). Particularly, sea-level rise further accelerated to a mean rate of ~15 mm yr^{-1} during 9–8 cal. kyr BP and reached ~30 mm yr^{-1} at 8.5–8.3 cal. kyr BP (Wang et al., 2013). Therefore, accommodation space in the river mouth should have seen a large increase from stage I to stage II owing to the inundation of the coastal plain and estuary mouth shoal (Fig. 8b–d). This resulted in an imbalance between sea-level rise and sediment supply in spite of a very strong summer monsoon at that time (Figs. 9b, 10). In addition, it has been reported that accelerated sea-level rise invariably leads to a nonlinear increase in tidal energy in river mouth systems (cf. Pethick and Orford, 2013), which could have led to a significant reduction in sediment trapping rate, or even a destructive phase during stage II (Table 2). Similar reports of sudden sea-level rise associated with rapid retreats of river mouth systems at ~9–8 cal. kyr BP have been made for various river mouths across the world (Hori and Saito, 2007; Tamura et al., 2009; Hijma and Cohen, 2010; Tjallingii et al., 2014), suggesting that system regime shift and erosional events could have taken place across a wide area at this time.

The second factor, a change in the shape of the river mouth induced by sea-level rise, could have contributed to system regime shift and the strengthening of marine processes in stage II (Figs. 8b–d, 10). Before 10 cal. kyr BP, the sheltered and elongated river mouth produced a strong downstream freshwater transport and a weak upstream tidal flow (Fig. 10a); this resulted in a fluvial-dominant state and the construction of both a widespread tidal flat in the inner estuary and a large mouth shoal (Figs. 5, 8). But in the open and broadened estuary during the 10 to 8 cal. kyr BP period, fluvial flow weakened, and both wave and tidal energy increased (Fig. 10b). The tidal flat of this more open estuary was therefore more vulnerable to wave (including storm)-induced erosion. An increase in the volume of the estuary's tidal prism seems very likely owing to the change in river mouth shape (Savenije, 2005). Thus the tidal range was amplified and the tidal current velocity would have been significantly greater in the paleo-estuary (Fig. 10b). Such an increase in tidal energy had been simulated by Uehara et al. (2002). The strengthened tidal currents reworked the estuary floor and formed the tidal trough (Uehara et al., 2002; Uehara and Saito, 2003; Feng et al., 2017). In addition, the submerged late Pleistocene terrace of the inner estuary (Fig. 9c) would have reduced the cross-sectional area of the tidal intrusion by approximately 50–75% according to the paleo-

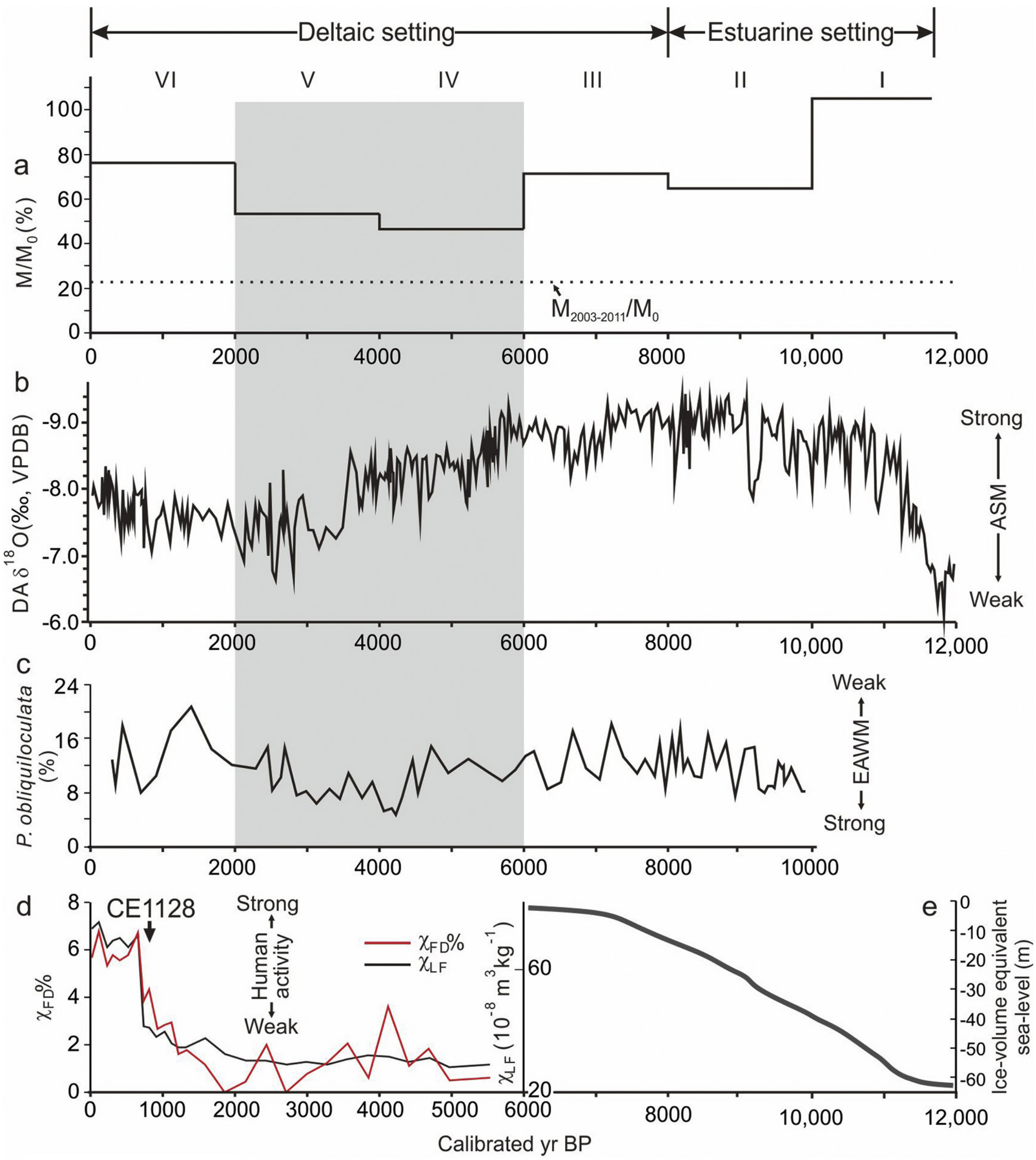

Fig. 9. (a) Comparison of the sediment budget on the millennial scale with that of very recent history. M represents the annual sediment mass deposited for each stage (Table 1). M_0 represents the annual sedimentation for the period 1958–1978. (b) the Asian Summer Monsoon (Dykoski et al., 2005), (c) the East Asian Winter Monsoon (Jian et al., 2000), (d) human activity (Wang et al., 2011) and (e) and ice-volume equivalent sea level (Lambeck et al., 2014). The y-axes represent (b) stable isotope of oxygen from the Dongge Cave, China, (c) the abundance of P. obliquiloculata which is an indicator for the strength of the Kuroshio Current, (d) magnetic susceptibility (χ_{LF}) and frequency-dependent magnetic susceptibility (χ_{FD}%) in the sediments of subaqueous Yangtze delta. These two parameters represent rock and soil erosion, respectively. Shaded area represents the obvious reduction in sediment trapping rate during stage IV and V, coupled with the weakening of summer monsoon and strengthening of winter monsoon. CE1128 refers to the time of increase in soil and rock erosion in the Yangtze drainage basin and an anthropogenic southward shift of the Yellow River, both induced by the war between the Song dynasty and the northern Liao nomads (Wang et al., 2011; Chen et al., 2012). (For interpretation of the references to colour in this figure legend, the reader is referred to the web version of this article.)

topography. Therefore, the only mechanism for maintaining the larger tidal prism is through high-speed tidal currents (Fig. 10b). This inference explains the location of the large tidal inlet at the head of the paleo-estuary, emplaced in the upstream region of the late Pleistocene terrace (Fig. 8c). Although the trough could have been a channel before 10 cal. kyr BP, we suggest that the bank slides and cross-bedded sand deposits detected in the trough-floor successions in core TZ at ~9.3–8.3 cal. kyr BP (Figs. 5d, 6h–k) are evidence for a high-speed tidal current at that time. We further speculate that the tidal inlet detected in core HM after 10.3 cal. kyr BP (Fig. 5b) was formed through similar processes, as it was located in the upstream region of the estuary mouth shoal (Fig. 8b).

An analogue of this kind of tidal trough can be found along the northern bank of present-day Hangzhou Bay, located to the south of the Yangtze River mouth (Fig. 1b; Xie et al., 2009). The formation of a large-scale tidal channel system (> 50 km long, 10 km wide, maximum depth > 50 m) in that location is thought to be due to the convergence of strong flood currents in the funnel-shaped estuary and the interfering effect of islands, both of which resulted in the strong erosion in the tidal trough. Numeric modelling suggests that a tidal channel system similar to that in Hangzhou Bay can be be constructed over a period of about 30 years (Xie et al., 2009). We therefore propose that the significant trough at the head of Yangtze estuary during the early Holocene (Fig. 5e) was a large-scale tidal inlet that resulted from sea-level rise, the funnel shape of the estuary, and the hindering effect of the late Pleistocene terrace (Fig. 10b).

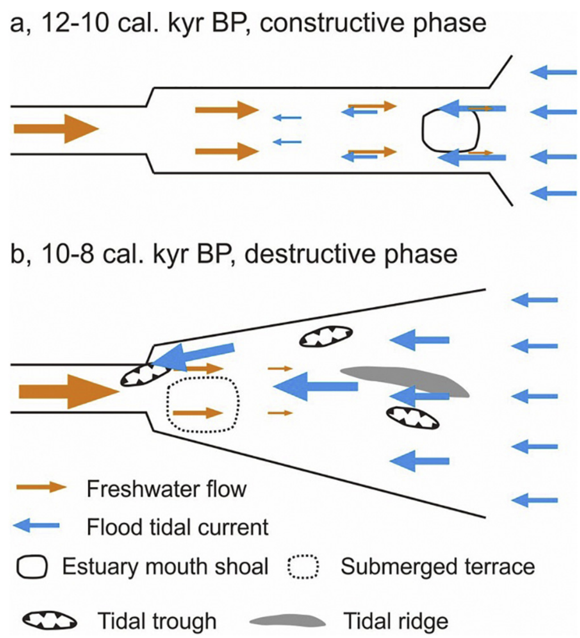

Fig. 10. Schematic diagram comparing the morphology and hydrodynamics in the Yangtze estuary as it changed from a constructive phase at 12–10 cal. kyr BP (a) to a destructive phase from 10 to 8 cal. kyr BP (b). Incoming tidal currents weakened rapidly because of friction, while fluvial flow remained relatively strong in the elongated estuary at 12 to 10 cal. kyr BP. In contrast, from 10 to 8 cal. kyr BP, fluvial flow dissipated rapidly because of the open funnel-shaped river mouth, while tidal currents strengthened landward in the narrowing estuary. Tidal trough and ridge structures developed in the funnel-shaped estuary owing to the strong tidal currents. Size of the arrow indicates the intensity of the flow or currents.

Finally, the tidal ridge-and-trough system buried under deltaic deposits and revealed by this study (Fig. 5d) also points to strong tidal functions in the offshore region after ~10 cal. kyr BP. Stratigraphic records show that the tidal ridge in this location was formed via the reshaping of the submerged estuary mouth shoal. Evidence for this is seen in the long period of sediment reworking on top of the sand ridge and erosion or depositional hiatus in the tidal trough from 10 to 6 cal. kyr BP (Figs. 5b, d, 6d–g). A strong tidal-current field has been simulated for the offshore paleo-Yangtze estuary, and this was favorable to the formation of a tidal ridge-and-trough system under early to mid-Holocene conditions (Uehara et al., 2002). Previous studies have also reported mud ridges in the inner shelf of ECS and sand ridges on the outer shelf, most likely formed by the reworking processes of strong tidal currents during the post-glacial transgression (Fig. 3; Liu et al., 1998; Chen et al., 2003; Feng et al., 2017). A landward migration of this kind of tidal ridge system was simulated coupled with the Holocene sea-level rise and the modeled system reached the present-day subaqueous valley off the Yangtze River mouth when sea level rose to approximately −45 m (Uehara et al., 2002). The presence of a buried tidal ridge-and-trough system in the present-day delta region thus indicates further landward migration of this strong offshore tidal-current field, caused by sea-level rise and the landward retreat of the river mouth system between 10 and 6 cal. kyr BP (Fig. 8b–e). Chrono-stratigraphy shows that the buried ridges stopped developing ~6000 years ago (Fig. 5b, e) when sea level approached its present height (Bard et al., 1996), further supporting the role of sea-level rise in its formation.

5.2. Mechanism for the changes in sediment trapping rate over past 8000 years

The significant decline in sediment trapping rate in the river mouth from stage I to stage II (Fig. 9a) was triggered by an erosion-dominated

Table 3
A comparison of major factors controlling the sediment trapping rate and the response of deposition or erosion at the river mouth in stages I-VI during the Holocene. The rate of ice-equivalent sea-level rise was calculated from Lambeck et al. (2014).

Stage	Time period (cal. kyr BP)	Mean annual sediment mass (10^6 t yr^{-1})	Rate of ice-equivalent sea-level rise (m kyr^{-1})	River mouth shape	Summer monsoon and freshwater and sediment discharge	Winter monsoon and resuspension of the subaqueous delta	Human impact	Response of the river mouth
I	11.7–10	224	11	Elongated and sheltered	From weak to strong	Unknown	Undetected	Development of the tidal river and tidal flat
II	10–8	137	12.5	Funnel-shaped	Strong	Weak	Undetected	System regime shift to a destructive phase
III	8–6	151	6	Funnel-shaped	Strong	Weak	Undetected	Delta initiation
IV	6–4	99	0.7	Funnel-shaped	Declined	Strong	Weak	Retreat of the subaqueous delta
V	4–2	113	0.4	Funnel-shaped	Weak	Strong	Weak	Seaward progradation
VI	2–0	162	0.1	Funnel-shaped	Weak	Weak	Intensified[a]	Enhanced seaward advance

[a] This included the artificial southward shift of the Yellow River mouth at CE1128.

state during stage II, owing to a rapid sea-level rise and the associated system regime shift as discussed above (Fig. 10; Table 3). A deltaic setting was established in stage III and changes in annual sedimentation along the Yangtze delta coast over the past 8000 years (stage III–VI) reflect changes in the strength of the Asian monsoon and human activities in the Yangtze River drainage basin (Fig. 9; Table 3). Another factor that may play a role in these sedimentation calculations is the possible southward dispersal of suspended sediment eroded from the abandoned Yellow River mouth in the north (Fig. 3).

The sediment trapping rate recovered slightly during stage III (8–6 cal. kyr BP; Fig. 9a) corresponding to the delta initiation at ~ 8 cal. kyr BP, a strong summer monsoon (Fig. 9b), and the rapid infilling of the delta apex (Fig. 8d, e). Subsequently, the trapping efficiency declines dramatically after about 6 cal. kyr BP. This corresponds to a decline in ASM strength at that time (Fig. 9b), leading to a decline in freshwater discharge into the river mouth evidenced by the increase in the marine-sourced organic carbon in the subaqueous sediment sequence (Zhan et al., 2012). We suggest that this decline in freshwater discharge weakened the fluvial depositional processes at the Yangtze River mouth, and this would be an important cause for the significant retreat of the subaqueous delta at that time (Figs. 5e, 7; Table 3). In addition, a strengthened winter monsoon during 4.6 to 2.7 cal. kyr BP (Fig. 9c; Jian et al., 2000; Xiao et al., 2006) could also account for the reduction in sediment trapping rates in stages IV and V. Under a strong winter monsoon additional sediments could be resuspended from the delta and transported southward to contribute to the formation of the longshore mud wedge shaped by the coastal current (Fig. 3; Xiao et al., 2006). The amount of southward dispersal of Yangtze suspended sediment has been estimated to be ~32% of the total sediment load discharged into the river mouth over the past 7000 years (Liu et al., 2007). This rate could have been significantly higher when the winter monsoon strengthened in stages IV and V, as evidenced by the higher sedimentation rate during the 6 to 3 cal. kyr BP period in the depocenter of the longshore mud wedge (Xu et al., 2012).

The clear increase in sediment trapping rate during stage VI (2–0 cal. kyr BP; Fig. 9a) cannot be explained by monsoon climate variability because the summer monsoon precipitation increased only slightly in the most recent few hundred years (Wang et al., 2005), and the winter monsoon weakened overall, but was also extremely variable (Fig. 9c; Jian et al., 2000). In contrast, this increase corresponds well with the increase in human activities (Fig. 9d) in the catchment, where it has been argued that over past ~2000 years expansion of the human population and changes in land-use increased erosion in the Yangtze drainage basin significantly (Wang et al., 2011). In addition, sediment reworked from the abandoned Yellow River mouth (Fig. 3) could have contributed to the sedimentation in the subaqueous Yangtze delta over the past few hundred years (Liu et al., 2010). The Yellow River was artificially shifted to a location north of the modern Yangtze River mouth during a war in CE 1128; it reverted to its present location, flowing into the Bohai Sea, in CE 1855 (Fig. 3; Chen et al., 2012). The amount of suspended sediment eroded from the abandoned Yellow River mouth after AD1855 has been estimated to be ~500 Mt yr^{-1}, which dispersed to the coastal zone and shelf of the south Yellow Sea (Saito et al., 1994). Although there is a huge radial tidal sand ridge system separating the abandoned Yellow River mouth from the Yangtze Delta (Fig. 3), part of this Yellow River sediment can still reach the Yangtze Delta. For example, Liu et al. (2010) have identified a Yellow River sediment signature in the subaqueous Yangtze delta sequence over the past 600 years. Thus the increase in sediment trapping rate during stage VI should be attributed to both intensified human activity in the Yangtze drainage basin and the southward migration of the Yellow River in CE 1128.

5.3. An evaluation of the present-day status of the Yangtze River mouth

Dramatic changes in sediment accumulation rate have taken place in the Yangtze Delta over the last 60 years (Table 2). Particularly notable are the changes in sediment accumulation rate, the annual sediment accumulation after 2003 (i.e. after completion of the TGD) is much lower than the lowest accumulation calculated for any time in the Holocene (stage IV, 6–4 cal. kyr BP; Fig. 9a) and the recent report of net erosion of ~638 Mt yr^{-1} in 2011–2013 (Li et al., 2015) is astonishing. It is possible that deposition after 2003 has been underestimated because of the short observational period. Even so, these decadal and annual changes still represent rapid responses to the changes in the Yangtze sediment load, which has declined to 136 Mt yr^{-1} since 2003 (Fig. 2). The average annual Yangtze sediment load may have been as low as ~146–166 Mt during 6–2 cal. kyr BP if we use a value of 68% for the mean trapping efficiency (Liu et al., 2007) of the annual sediment mass at the river mouth (Table 2). We therefore hypothesize that the post-2003 Yangtze sediment load is below its 'natural' level and the Yangtze Delta has experienced a transition to a sediment-starved state. A retreat of the subaqueous delta occurred as a response to a reduction in freshwater discharge and sediment load induced by monsoon decline after ~6 cal. kyr BP (Fig. 7; Table 3), which could provide an analogue for the present-day sediment-starved situation. The erosion observed in the subaqueous delta in recent years (Table 2; Yang et al., 2011; Li et al., 2015) could be evidence of its ongoing retreat.

The Yangtze River mouth system changed from a constructive to a destructive phase mainly owing to the acceleration of sea-level rise during 10–8 cal. kyr BP, as discussed in Section 5.1. This could also be an analogue for the Yangtze Delta in the near future as the sea-level rise is predicted to accelerate to a rate of 5–13 mm yr^{-1} by 2100 (Kopp et al., 2016). Together with the fact that its present-day sediment input is far below early Holocene levels (Figs. 2, 9), an imbalance between sediment input and sea-level rise is clearly foreseeable.

Additionally, coastal engineering (Fig. 1c), which 'hardened' the shoreline of the Yangtze Delta could also intensify coastal erosion in the situation of a rapid sea-level rise. It has been reported that the reclamation and embankment of approximately 1100 km^2 of intertidal land has induced accelerated erosion in the subtidal zone since the mid-1990s (Du et al., 2016). The Qingcaosha Reservoir and the embankment of the Hengsha Shoal (Fig. 1c) also used a large area of the intertidal and subtidal land. These coastal engineering projects significantly reduced space for flood water management. Particularly when coupled with sea-level rise, these embanked river mouth shoals will enhance erosion in the tidal channels in a way that is similar to the role played by the late Pleistocene terrace in the early Holocene estuary (Figs. 8c, 10).

6. Conclusions

Millenial-scale records of stratigraphic architecture and sedimentary discontinuities from delta-wide stratigraphic cross-sections, reconstructed paleo-topographic maps, and sediment trapping rate calculations in the Yangtze River mouth give us an image of the three-dimensional evolution of the Yangtze River mouth during the Holocene. Observed sedimentary history were controlled by sea-level change, Asian monsoon dynamics, basal topography, and human activity. Several conclusions can be drawn from this data:

1. The Yangtze River mouth changed from a constructive to a destructive phase from 12 to 10 cal. kyr BP to 10–8 cal. kyr BP owing to the acceleration of sea-level rise and associated change in river mouth shape. In the latter stage, sedimentary discontinuities characterize the sedimentary sequences, formed by erosion and sediment reworking. Change in the river mouth shape, coupled with sea-level rise promoted the strengthening of marine processes between 10 and 8 cal. kyr BP.
2. A distinct tidal inlet, ~30 m deep, occurred at the head of paleo-Yangtze estuary, which we suggest was the result of high-energy tidal currents restricted and focused by the late Pleistocene terrace

in the inner estuary during a period of rapid sea-level rise.

3. A tidal ridge-and-trough system occurred in the offshore valley of the paleo-Yangtze River mouth during the 10 to 6 cal. kyr BP period; this was coupled with sea-level rise and the landward retreat of the river mouth system.
4. The subaqueous delta retreated landward as a response to the decline in sediment supply induced by summer monsoon weakening after 6 cal. kyr BP.
5. The sediment trapping rate in the Yangtze Delta over past 8000 years changed primarily in response to changes in the Asian monsoon and human activities. A low trapping rate occurred between 6 and 2 cal. kyr BP when summer monsoon declined and winter monsoon strengthened. The high sediment trapping rate over the past 2000 years was induced by the intensified human activity in the Yangtze drainage basin and the anthropogenic southward shift of the Yellow River mouth.
6. The sediment trapping rate has declined to the lowest level in the Yangtze Delta's history as a response to the severe decline in sediment supply since the completion of the TGD. An increase in coastal erosion and a shift towards a new equilibrium between erosion and deposition in relation to delta morphology is foreseeable in the near future due to both the sediment supply shortage and predicted sea-level rise. Because embankment is the only method currently in use for present-day coastal protection, and this method leads to greater coastal erosion under conditions of sea-level rise, we strongly urge managers to employ long-term monitoring and search for strategies to mitigate the threats of coastal erosion for the densely populated Yangtze delta.

Acknowledgments

This study was jointly supported by the National Natural Science Foundation of China (Grant No. 41576042), the Ministry of Science and Technology of China (Grant No. SKLEC-2012KYYW01), National Key Research Programme (Grant No. 2016YFC0402600) and the Ministry of Land and Resources of Public Welfare Scientific Research of China (Grant No. 201211009). Authors are grateful to two anonymous reviewers for their constructive comments and to Drs Brian Finlayson and David Dettman who helped edit the manuscript.

Appendix A. Supplementary data

Supplementary data to this article can be found online at https://doi.org/10.1016/j.earscirev.2018.08.012.

References

Bard, E., Hamelin, B., Arnold, M., Montaggioni, L., Cabioch, G., Faure, G., Rougerie, F., 1996. Deglacial sea-level record from Tahiti corals and the timing of global meltwater discharge. Nature 382, 241–244.

Beardsley, R.C., Limeburner, R., Yu, H., Cannon, G.A., 1985. Discharge of the Changjiang (Yangtze River) into the East China Sea. Cont. Shelf Res. 4, 57–76.

Bøtter-Jensen, L., Andersen, C.E., Duller, G.A.T., Murray, A.S., 2003. Developments in radiation, stimulation and observation facilities in luminescence measurements. Radiat. Meas. 37, 535–541.

Chang, P., Isobe, A., 2003. A numerical study on the Changjiang diluted water in the Yellow and East China Seas. J. Geophys. Res. 108, 3299. https://doi.org/10.1029/2002JC001749.

Changjiang Water Resources Commission, 1999. Atlas of the Changjiang River basin. Atlas Press in China, Beijing (in Chinese).

Chen, J.Y., Shen, H.T., Yun, C.X., 1988. Dynamic Processes and Morphological Evolution of Yangtze Estuary. Shanghai Science and Technology Press, Shanghai 453 pp. (in Chinese, with English summary).

Chen, Z., Song, B., Wang, Z., Cai, Y., 2000. Late Quaternary evolution of the subaqueous Yangtze Delta, China: sedimentation, stratigraphy, palynology, and deformation. Mar. Geol. 162, 423–441.

Chen, Z., Saito, Y., Hori, K., Zhao, Y., Kitamura, A., 2003. Early Holocene mud-ridge formation in the Yangtze offshore, China: a tidal-controlled estuarine pattern and sea-level implications. Mar. Geol. 198, 245–257.

Chen, Q., Li, C., Li, P., Liu, B., Sun, H., 2008. Late Quaternary palaeosols in the Yangtze delta, China, and their palaeoenvironmental implications. Geomorphology 100, 465–483.

Chen, Y., Syvitski, J.P.M., Gao, S., Overeem, I., Kettner, A.J., 2012. Socio-economic impacts on flooding: a 4000-year history of the Yellow River, China. Ambio 41, 682–698.

Chen, T., Wang, Z., Wu, X., Gao, X., Li, L., Zhan, Q., 2015. Magnetic properties of tidal flat sediments on the Yangtze coast, China: early diagenetic alteration and implications. The Holocene 25, 832–843.

Coleman, J.M., Roberts, H.H., Stone, G.W., 1998. Mississippi river delta: and overview. J. Coast. Res. 14, 698–716.

Dai, Z., Liu, J.T., Wei, W., Chen, J., 2014. Detection of the Three Gorges Dam influence on the Changjiang (Yangtze River) submerged delta. Sci. Rep. 4, 6600. https://doi.org/10.10-38/srep06600.

Dalrymple, R.W., Choi, K., 2007. Morphologic and facies trends through the fluvial-marine transition in tide-dominated depositional systems: a schematic framework for environmental and sequence-stratigraphic interpretation. Earth Sci. Rev. 81, 135–174.

Day Jr., J.W., Boesch, D.F., Clairain, E.J., Kemp, G.P., Laska, S.B., Mitsch, W.J., Orth, K., Mashriqui, H., Reed, D.J., Shabman, L., Simenstad, C.A., Streever, B.J., Twilley, R.R., Watson, C.C., Wells, J.T., Whigham, D.F., 2007. Restoration of the Mississippi Delta: lessons from Hurricanes Katrina and Rita. Science 315, 1679–1684.

Du, J.-L., Yang, S.-L., Feng, H., 2016. Recent human impacts on the morphological evolution of the Yangtze River delta foreland: a review and new perspectives. Estuar. Coast. Shelf Sci. 181, 160–169.

Dykoski, C.A., Edwards, R.L., Cheng, H., Yuan, D., Cai, Y., Zhang, M., Lin, Y., Qing, J., An, Z., Revenaugh, J., 2005. A high-resolution, absolute-dated Holocene and deglacial Asian monsoon record from Dongge Cave, China. Earth Planet. Sci. Lett. 233, 71–86.

Ensing, E., de Swart, H.E., Schuttelaars, H.M., 2015. Sensitivity of tidal motion in well-mixed estuaries to cross-sectional shape, deepening, and sea level rise. Ocean Dyn. 65, 933–950.

Feng, Z., Liu, B., Zhao, Y., Li, X., Dada, O.A., Jiang, L., Si, S., 2017. Structure, distribution, and evolution history of the Early Holocene erosional mud ridge system on the inner East China Sea shelf near the Yangtze River estuary. Geomorphology 283, 173–188.

Giosan, L., Syvitski, J., Constantinescu, S., Day, J., 2014. Protect the world's deltas. Nature 516, 31–33.

Hijma, M.P., Cohen, K.M., 2010. Timing and magnitude of the sea-level jump preluding the 8200 yr event. Geology 38, 275–278.

Holleman, R.C., Stacey, M.T., 2014. Coupling of sea level rise, tidal amplification, and inundation. J. Phys. Oceanogr. 44, 1439–1455.

Hori, K., Saito, Y., 2007. An early Holocene sea-level jump and delta initiation. Geophys. Res. Lett. 34, L18401. https://doi.org/10.1029/2007GL031029.

Hori, K., Saito, Y., Zhao, Q., Cheng, X., Wang, P., Sato, Y., Li, C., 2001. Sedimentary facies of the tide-dominated paleo-Changjiang (Yangtze) estuary during the last transgression. Mar. Geol. 177, 331–351.

Hori, K., Saito, Y., Zhao, Q., Wang, P., 2002a. Evolution of the coastal depositional systems of the Changjiang (Yangtze) River in response to late Pleistocene-Holocene sea-level changes. J. Sediment. Res. 72, 884–897.

Hori, K., Saito, Y., Zhao, Q., Wang, P., 2002b. Architecture and evolution of the tide-dominated Changjiang (Yangtze) River delta, China. Sediment. Geol. 146, 249–264.

Hsiung, K.-H., Saito, Y., 2017. Sediment trapping in deltas of small mountainous rivers of southwestern Taiwan and its influence on East China Sea sedimentation. Quat. Int. 455, 30–44.

Hu, D.K., Clift, P.D., Boning, P., Hannigan, R., Hillier, S., Blusztajn, J., Wan, S.M., Fuller, D.Q., 2013. Holocene evolution in wreathing and erosion patterns in the Pearl River delta. Geochem. Geophys. Geosyst. 14, 2349–2368.

Isobe, A., 2008. Recent advances in ocean-circulation research on the Yellow Sea and east China Sea shelves. J. Oceanogr. 64, 569–584.

Jian, Z., Wang, P., Saito, Y., Wang, J., Pflaumann, U., Oba, T., Cheng, X., 2000. Holocene variability of the Kuroshio Current in the Okinawa Trough, northwestern Pacific Ocean. Earth Planet. Sci. Lett. 184, 305–319.

Kong, G.S., Lee, C.W., 2005. Marine reservoir corrections (ΔR) for southern coastal waters of Korea. Sea J. Korean Soc. Oceanogr. 10, 124–128.

Kopp, R.E., Kemp, A.C., Bittermann, K., Horton, B.P., Donnelly, J.P., Gehrels, W.R., Hay, C.C., Mitrovica, J.X., Morrow, E.D., Rahmstorf, S., 2016. Temperature-driven global sea-level variability in the Common Era. Proc. Natl. Acad. Sci. U. S. A. 113, E1434–E1441. https://doi.org/10.1073/pnas.1517056113.

Lambeck, K., Rouby, H., Purcell, A., Sun, Y., Sambridge, M., 2014. Sea level and global ice volumes from the Last |Glacial Maximum to the Holocene. PNAS 111, 15296–15303. https://doi.org/10.1073/pnas.1411762111.

Li, C., Wang, P., 1998. Late Quaternary stratigraphy of the Changjiang River mouth. Science Press, Beijing (222 pp.).

Li, C., Zhang, G., 1996. The unconformity and diastems in the postglacial sequence in the Changjiang Delta and Qiantangjiang Estuary. Prog. Nat. Sci. 6, 206–216.

Li, C., Chen, Q., Zhang, J., Yang, S., Fan, D., 2000. Stratigraphy and paleoenvironmental changes in the Yangtze Delta during the Late Quaternary. J. Asian Earth Sci. 18, 453–469.

Li, Z., Song, B., Saito, Y., Li, J., Li, Z., Lu, A., 2009. Sedimentary facies and geochemical characteristics of Jiangdou core JD01 from the upper delta plain of Changjiang (Yangtze) Delta. China. In: Amorosi, A. (Ed.), Proceedings of the 27th IAS Meeting of Sedimentologists. Medimond, Bologna (Italy), pp. 55–65.

Li, M., Chen, Z., Yin, D., Chen, J., Wang, Z., Sun, Q., 2011. Morphodynamic characteristics of the dextral diversion of the Yangtze River mouth, China: tidal and the Coriolis Force controls. Earth Surf. Process. Landf. 36, 641–650.

Li, G., Li, P., Liu, Y., Qiao, L., Ma, Y., Xu, J., Yang, Z., 2014. Sedimentary system response to the global sea level change in the East China Seas since the last glacial maximum. Earth Sci. Rev. 139, 390–405.

Li, B., Yan, X.X., He, Z.F., Chen, Y., Zhang, J.H., 2015. Impacts of the Three Gorges Dam

on the bathymetric evolution of the Yangtze River Estuary. Chin. Sci. Bull. 60, 1735–1744. https://doi.org/10.1360/N972014-01074. (in Chinese).
Liu, Z.X., Xia, D.X., Berné, S., Wang, K.Y., Marsset, T., Tang, Y.X., Bourillet, J.F., 1998. Tidal deposition systems of China's continental shelf, with special reference to the eastern Bohai Sea. Mar. Geol. 145, 225–253.
Liu, J.P., Li, A.C., Xu, K.H., Velozzi, D.M., Yang, Z.S., Milliman, J.D., DeMaster, D.J., 2006. Sedimentary features of the Yangtze River-derived along-shelf clinoform deposit in the East China Sea. Cont. Shelf Res. 26, 2141–2156.
Liu, J.P., Xu, K.H., Li, A.C., Milliman, J.D., Velozzi, D.M., Xiao, S.B., Yang, Z.S., 2007. Flux and fate of Yangtze River sediment delivered to the East China Sea. Geomorphology 85, 208–224. https://doi.org/10.1016/j.geomorph.2006.03.023.
Liu, J., Saito, Y., Kong, X., Wang, H., Xiang, L., Wen, C., Nakashima, R., 2010. Sedimentary record of environmental evolution off the Yangze River estuary, East China Sea, during the last ~13,000 years, with special reference to the influence of the Yellow River on the Yangtze River delta during the last 600 years. Quat. Sci. Rev. 29, 2424–2438.
Lu, X., Higgitt, D.L., 1998. Recent changes of sediment yield in the upper Yangtze, China. Environ. Manag. 22, 697–709.
Milliman, J.D., Shen, H.-T., Yang, Z.-S., Meade, R.H., 1985. Transport and deposition of river sediment in the Changjiang estuary and adjacent continental shelf. Cont. Shelf Res. 4, 37–45.
Nageswara Rao, K., Saito, Y., Nagakumar, K.C.V., Demudu, G., Rajawat, A.S., Kubo, S., Li, Z., 2015. Palaeogeography and evolution of the Godavari delta, east coast of India during the Holocene: an example of wave-dominated and fan-delta settings. Palaeogeogr. Palaeoclimatol. Palaeoecol. 440, 213–233.
Nerem, R.S., Beckley, B.D., Fasullo, J.T., Hamlington, B.D., Masters, D., Mitchum, G.T., 2018. Climate-change-driven accelerated sea-level rise detected in the altimeter era. Proc. Natl. Acad. Sci. U. S. A. https://doi.org/10.1073/pnas.1717312115.
Nian, X.M., Chen, F.Y., Li, F., Gao, X., 2015. Optical dating of a Paleolithic site near the eastern coastal region of Shandong, northern China. Quat. Geochronol. 30, 466–471.
Nian, X., Zhang, W., Wang, Z., Sun, Q., Chen, J., Chen, Z., 2018a. Optical dating of Holocene sediments from the Yangtze River (Changjiang) Delta, China. Quat. Int. 467, 251–263.
Nian, X., Zhang, W., Wang, Z., Sun, Q., Chen, J., Chen, Z., Hutchinson, S.M., 2018b. The chronology of a sediment core from incised valley of the Yangtze River delta: comparative OSL and AMS ^{14}C dating. Mar. Geol. 395, 320–330.
Pan, D., Chen, T., Zhan, Q., Wang, Z., 2017. Mineral magnetic properties of Holocene sediments in the subaqueous Yangtze delta and the implications for human activity and early diagenesis. Quat. Int. 459, 133–143.
Pethick, J., Orford, J.D., 2013. Rapid rise in effective sea-level in southwest Bangladesh: its causes and contemporary rates. Glob. Planet. Chang. 111, 237–245.
Posamentier, H.W., Allen, G.P., 1999. Siliciclastic sequence stratigraphy—concepts and applications. SEPM Concepts Sedimentol. Paleontol. 7 (210 pp.).
Saito, Y., Ikehara, K., Katayama, H., Matsumoto, E., Yang, Z., 1994. Course shift and sediment-discharge changes of the Huanghe recorded in sediments of the East China Sea. Chishitsu News 476, 8–16.
Savenije, H.H.G., 2005. Salinity and Tides in Alluvial Estuaries. Elsevier, New York (194 pp.).
Song, B., Li, Z., Saito, Y., Okuno, J., Li, Z., Lu, A., Hua, D., Li, J., Li, Y., Nakashima, R., 2013. Initiation of the Changjiang (Yangtze) delta and its response to the mid-Holocene sea level change. Palaeogeogr. Palaeoclimatol. Palaeoecol. 388, 81–97.
Southon, J., Kashgarian, M., Fontugne, M., Metivier, B., Yim, W.W.-S., 2002. Marine reservoir corrections for the Indian Ocean and Southeast Asia. Radiocarbon 44, 167–180.
Stanley, D.J., Chen, Z.Y., 2000. Radiocarbon dates in China's Holocene Yangtze delta: record of sediment storage and reworking, not timing of deposition. J. Coast. Res. 16, 1126–1132.
Stanley, D.J., Warne, A.G., 1994. Worldwide initiation of Holocene marine deltas by deceleration of sea-level rise. Science 265, 228–231.
Stanley, D.J., Warne, A.G., 1998. Nile delta in its destruction phase. J. Coast. Res. 14, 794–825.
Stuiver, M., Reimer, P.J., Reimer, R., 2015. CALIB: Radiocarbon Calibration. http://calib.qub.ac.uk/calib/ (September 2015).
Syvitski, J.P.M., Kettner, A.J., Overeem, I., Hutton, E.W.H., Hannon, M.T., Brakenridge, G.R., Day, J., Vorosmarty, C., Saito, Y., Giosan, L., Nicholls, R.J., 2009. Sinking deltas due to human activities. Nat. Geosci. 2, 681–686. https://doi.org/10.1038/ngeo629.
Tamura, T., Saito, Y., Sieng, S., Ben, B., Kong, M., Sim, I., Choup, S., Akiba, F., 2009. Initiation of the Mekong River delta at 8 ka: evidence from the sedimentary succession in the Cambodian lowland. Quat. Sci. Rev. 28, 327–344.
Tanabe, S., Saito, Y., Vu, Q.L., Hanebuth, T.J.J., Ngo, Q.L., Kitamura, A., 2006. Holocene evolution of the Song Hong (Red River) delta system, northern Vietnam. Sediment. Geol. 187, 29–61.
Tjallingii, R., Stattegger, K., Wetzel, A., Phach, P.V., 2010. Infilling and flooding of the Mekong River incised valley during deglacial sea-level rise. Quat. Sci. Rev. 29, 1432–1444.
Tjallingii, R., Stattegger, K., Stocchi, P., Saito, Y., Wetzel, A., 2014. Rapid flooding of the southern Vietnam shelf during the early to mid-Holocene. J. Quat. Sci. 29, 581–588.
Uehara, K., Saito, Y., 2003. Late quaternary evolution of the Yellow/East China Sea tidal regime and its impacts on sediments dispersal and seafloor morphology. Sedim. Geol. 162, 25–38.
Uehara, K., Saito, Y., Hori, K., 2002. Paleotidal regime in the Changjiang (Yangtze) Estuary, the East China Sea, and the Yellow Sea at 6 ka and 10 ka estimated from a numerical model. Mar. Geol. 182, 179–192.
Van Wagoner, J.C., Posamentier, H.W., Mitchum Jr., R.M., Vail, P.R., Sarg, J.F., Loutit, T.S., Hardenbol, J., 1988. An overview of the fundamentals of sequence stratigraphy and key definitions. In: Wilgus, C.K., Hastings, B.S., Kendall, C.G.St.C., Posamentier, H.W., Ross, C.A., Van Wagoner, J.C. (Eds.), Sea Level Changes—An Integrated Approach. 42. SEPM Special Publication, pp. 39–45.
Wang, P., Zhang, J., Zhao, Q., Min, Q., Bian, Y., Zheng, L., Cheng, X., Chen, R., 1988. Foraminifera and Ostracode in the Surficial Sediments of the East China Sea. Ocean Press, Beijing, pp. 52–113 (in Chinese).
Wang, Y., Cheng, H., Edwards, R.L., He, Y., Kong, X., An, Z., Wu, J., Kelly, M.J., Dykoski, C.A., Li, X., 2005. The Holocene Asian monsoon: links to solar changes and North Atlantic climate. Science 308, 854–857. https://doi.org/10.1026/science.1106296.
Wang, Z., Xu, H., Zhan, Q., Saito, Y., He, Z., Xie, J., Li, X., Dong, Y., 2010. Lithological and palynological evidence of late Quaternary depositional environments in the subaqueous Yangtze delta, China. Quat. Res. 73, 550–562.
Wang, Z., Li, M., Zhang, R., Liu, Y., Saito, Y., Xie, J., Li, B., Zhao, B., 2011. Impacts of human activity on the late Holocene development of the subaqueous Yangtze delta, China, as shown by magnetic properties and sediment accumulation rates. The Holocene 21, 393–408.
Wang, Y., Zhang, Y., Zou, X., Zhu, D., Piper, D., 2012a. The sand ridge field of the South Yellow Sea: origin by river-sea interaction. Mar. Geol. 291–294, 132–146.
Wang, Z., Zhuang, C., Saito, Y., Chen, J., Zhan, Q., Wang, X., 2012b. Early mid-Holocene sea-level change and coastal environmental response on the southern Yangtze delta plain, China: implications for the rise of Neolithic culture. Quat. Sci. Rev. 35, 51–62.
Wang, Z., Zhan, Q., Long, H., Saito, Y., Gao, X., Wu, X., Li, L., Zhao, Y., 2013. Early to mid-Holocene rapid sea-level rise and coastal response on the southern Yangtze delta plain, China. J. Quat. Sci. 28, 659–672.
Wintle, A.G., Murray, A.S., 2006. A review of quartz optically stimulated luminescence characteristics and their relevance in single-aliquot regeneration dating protocols. Radiat. Meas. 41, 369–391.
Woodruff, J.D., Irish, J.L., Camargo, S.J., 2013. Coastal flooding by tropical cyclones and sea-level rise. Nature 504, 44–52.
Xiao, S., Li, A., Liu, J.P., Chen, M., Xie, Q., Jiang, F., Li, T., Xiang, R., Chen, Z., 2006. Coherence between solar activity and the East Asian winter monsoon variability in the past 8000 years from Yangtze River-derived mud in the East China Sea. Palaeogeogr. Palaeoclimatol. Palaeoecol. 237, 293–304. https://doi.org/10.1016/j.palaeo.2005.12.003.
Xie, D., Wang, Z., Gao, S., De Vriend, H.J., 2009. Modeling the tidal channel morphodynamics in a macro-tidal embayment, Hangzhou Bay, China. Cont. Shelf Res. 29, 1757–1767.
Xu, K., Li, A., Liu, J.P., Milliman, J.D., Yang, Z., Liu, C.-S., Kao, S.-J., Wan, S., Xu, F., 2012. Provenance, structure, and formation of the mud wedge along inner continental shelf of the East China Sea: A synthesis of the Yangtze dispersal system. Mar. Geol. 291–294, 176–191. https://doi.org/10.1016/j.margeo.2011.06.003.
Xu, T., Shi, X., Wang, G., Qiao, S., Yang, G., Liu, S., Wang, X., Zhao, Q., 2013. Sedimentary facies of the subaqueous Changjiang River delta since the late Pleistocene. Chin. J. Oceanol. Limnol. 31, 1107–1119.
Xu, T., Wang, G., Shi, X., Wang, X., Yao, Z., Yang, G., Fang, X., Qiao, S., Liu, S., Wang, X., Zhao, Q., 2016. Sequence stratigraphy of the subaqueous Changjiang (Yangtze River) delta since the Last Glacial Maximum. Sediment. Geol. 331, 132–147.
Yang, S.Y., Li, C.X., Jung, H.S., Lee, H.J., 2002. Discrimination of geochemical compositions between the Changjiang and the Huanghe sediments and its application for the identification of sediment source in the Jiangsu coastal plain, China. Mar. Geol. 186, 229–241.
Yang, S.L., Milliman, J.D., Li, P., Xu, K., 2011. 50,000 dams later: erosion of the Yangtze River and its delta. Glob. Planet. Chang. 75, 14–20. https://doi.org/10.1016/j.gloplacha.2010.09.006.
Yang, S.L., Milliman, J.D., Xu, K.H., Deng, B., Zhang, X.Y., Luo, X.X., 2014. Downstream sedimentary and geomorphic impacts of the Three Gorges Dam on the Yangtze River. Earth Sci. Rev. 138, 469–486. https://doi.org/10.1016/j.earscirew.2014.07.006.
Yoneda, M., Uno, H., Shibata, Y., Suzuki, R., Kumamoto, Y., Yoshida, K., Sasaki, T., Suzuki, A., Kawahata, H., 2007. Radiocarbon marine reservoir ages in the western Pacific estimated by pre-bomb molluscan shells. Nucl. Inst. Methods Phys. Res. B 259, 432–437.
Yu, X., Zhan, Q., Wang, Z., 2016. Sedimentary structures and grain size patterns of the geomorphic units in the Yangtze River mouth. Mar. Geol. Quat. Geol. 36, 1–11 (in Chinese, with English abstract).
Zhan, Q., Wang, Z., Xie, Y., Xie, J., He, Z., 2012. Assessing C/N and δ13C as indicators of Holocene sea level and freshwater discharge changes in the subaqueous Yangtze delta, China. The Holocene 22, 697–704.
Zhang, X., Dalrymple, R.W., Lin, C.M., 2017. Facies and stratigraphic architecture of the late Pleistocene to early Holocene tide-dominated paleo-Changjiang (Yangtze River) delta. Geol. Soc. Am. Bull. 130, 455–483.
Zhao, B., Wang, Z., Chen, J., Chen, Z., 2008. Marine sediment records and relative sea level change during late Pleistocene in the Changjiang delta area and adjacent continental shelf. Quat. Int. 186, 164–172.
Zheng, G.Y., 1989. The Correlation and Comparison of Quaternary Stratigraphy in South Yellow Sea. Science Press, Beijing, pp. 9–180 (in Chinese).
Zong, Y., Lloyd, J.M., Leng, M.J., Yim, W.W.-S., Huang, G., 2006. Reconstruction of Holocene monsoon history from the Pearl River estuary, southern China, using diatoms and carbon isotope ratios. The Holocene 16, 251–263.
Zong, Y., Huang, K., Yu, F., Zheng, Z., Switzer, A., Huang, G., Wang, N., Tang, M., 2012. The role of sea-level rise, monsoonal discharge and palaeo-landscape in the early Holocene evolution of the Pearl River delta, southern China. Quat. Sci. Rev. 54, 77–88.